Journal of Materials Chemistry A

Accepted Manuscript

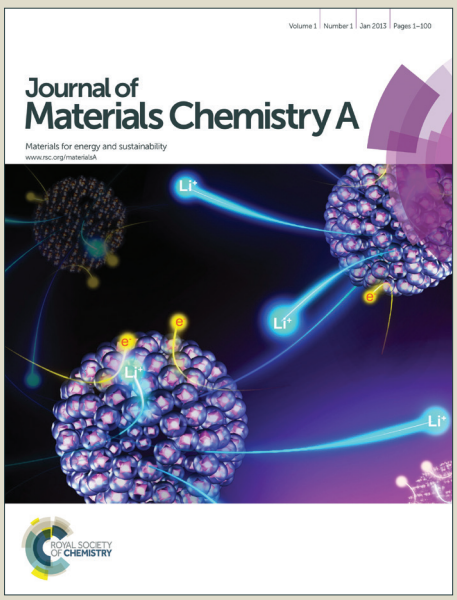

ROYAL SOCIETY OF CHEMISTRY

www.rsc.org/materialsA

Design and Control of Organic Semiconductors and Their Nanostructures for Polymer–Fullerene-Based Photovoltaic Devices

Tomokazu Umeyama[ab] and Hiroshi Imahori*[ac]

[a] *Department of Molecular Engineering, Graduate School of Engineering, Kyoto University, Nishikyo-ku, Kyoto, 615-8510, Japan*

[b] *PRESTO, Japan Science and Technology Agency (JST), 4-1-8 Honcho, Kawaguchi, Saitama 332-0012, Japan*

[c] *Institute for Integrated Cell-Material Sciences (WPI-iCeMS), Kyoto University, Nishikyo-ku, Kyoto 615-8510, Japan*

E-mail: imahori@scl.kyoto-u.ac.jp; Fax: +81-75-383-2571; Tel: +81-75-383-2566

Abstract

Polymer solar cell (PSC) technology has continued to be developed, and the power conversion efficiency (PCE) has now exceeded 10%. The rapid improvement of PCEs in the last decade has mainly resulted from versatile synthetic efforts for conjugated polymers as electron-donors and fullerene derivatives as electron-acceptors. This Feature Article highlights recent exploration of unique, attractive building blocks, i.e., quinoidal units, phospholes, porphyrins, and fluorinated aromatic rings, which can be incorporated into low bandgap conjugated polymers. As candidates for the next-generation acceptor materials that replace the benchmark acceptor, [6,6]-phenyl-C_{61}-butyric acid methyl ester ([60]PCBM), fullerene bisadduct regioisomers are also overviewed. Furthermore, we summarized recent attempts for the construction of one-dimensionally confined, organic donor–acceptor heterojunction nanorods and their applications to photovoltaic and optoelectronic devices. The topics in this article are not intended to cover an exhaustive list of PSC researches, but involve the fundamental aspect to stimulate further studies for getting new insights into structure–property relationship in PSC devices.

1. Introduction

Conversion of unlimited solar radiation into electricity has emerged as a highly promising solution for world increasing energy demands. Polymer solar cells (PSCs) have attracted a tremendous amount of research activity in the academic and industrial communities because of their potential advantages including low cost, light weight, and fast, economical roll-to-roll production compared to the currently market dominant crystalline silicon solar cells.[1-3] So far the most successful PSC devices to date are based on a bulk heterojunction (BHJ) structure, which typically has an interpenetrating bicontinuous network comprising of electron-donating conjugated polymers and electron-accepting fullerene derivatives.[4-6] The device structure of PSCs typically involves a photoactive layer with the BHJ structure sandwiched between an ITO bottom anode modified by poly(ethylene dioxythiophene) doped with polystyrene sulfonic acid (PEDOT:PSS) and a low-work function metal cathode such as Al to collect holes and electrons, respectively (Fig. 1). Calcium and titanium oxides have frequently been employed as an electron-transporting layer between the photoactive layer and Al electrode.[7] Recently, PSC devices with an inverted device structure, using an ITO bottom cathode and a high-work function metal anode, have also intensively been investigated owing to the long-term ambient stability (Fig. 1).[8-10] Careful choice of buffer layers between the photoactive layer and cathode/anode has improved power conversion efficiencies (PCEs) of the inverted devices, which become comparable with those of the conventional devices.[11-15]

Fig. 1

In PSC devices, the conversion of light-energy to electricity generally involves the following fundamental steps: 1) absorbing incident photons by the polymers or fullerene derivatives to form

excitons, 2) diffusion of the excitons to an interface of the polymer and fullerene, 3) dissociation of the excitons to form holes in the polymer and electrons in the fullerene derivative, 4) transportation of the separated charges toward the respective electrodes, and 5) charge collection at the electrodes. Note that three photovoltaic parameters determine the PCE of a solar cell device: short-circuit current density (J_{SC}), open-circuit voltage (V_{OC}), and fill factor (*FF*). The PCE is equal to the product of these parameters divided by the input power. The J_{SC} value of a solar cell depends on the efficiencies corresponding to the above 5 steps, and V_{OC} is mainly proportional to the energy level difference between HOMO of the electron-donor and LUMO of the electron-acceptor.[16,17] *FF* is related to series resistance (R_s) and shunt resistance (R_{sh}); lower R_s and higher R_{sh} lead to high *FF*.[18,19]

The maximum PCE of PSCs has increased recently to over 8% in single BHJ PSCs appeared in scientific literatures.[11-15,20-25] However, the necessity of over 15% PCE has been recognized for future commercialization. Therefore, state-of-the-art studies on PSCs still mainly lie on increasing the PCE. A lot of efforts have been paid to design and synthesize highly efficient photovoltaic conjugated polymer donor[26-30] and fullerene acceptor materials.[31-35] Indeed, the rapid improvement of the PCEs in the last decade has mainly resulted from versatile synthetic efforts for fine-tuning the electronic properties of the polymer donors. The ideal photovoltaic materials should have broad and intense absorption in visible and near-infrared region to harvest solar light efficiently for achieving high J_{SC} as well as suitable energy levels of HOMO and LUMO to facilitate the exciton dissociation at the polymer–fullerene interface with retaining the high V_{OC}.[16,17] These requirements are not independent of each other, i.e., raising the HOMO and/or lowering the LUMO lead to the smaller HOMO-LUMO bandgap, but the smaller V_{OC} stemming from the higher HOMO level of the polymer and/or the lower LUMO level of the fullerene. Therefore, it is essential to balance the conflicting parameters when modulating the electronic structure of the polymer for the high

photovoltaic performance. In addition, pivotal is optimizing morphology of the polymer–fullerene blend active layer with nano-sized phase separation of the interpenetrating network for achieving the high PCE.[36-39] Together with excellent charge separation (CS) and transport properties of fullerenes and fullerene derivatives due to their small reorganization energies of electron transfer (ET),[40,41] such nano-sized bicontinuous structure can promote exciton diffusion to the polymer–fullerene interface for efficient CS and subsequent favorable transport of the photogenerated charges, eventually maximizing the V_{OC}, J_{SC} and FF. High charge carrier mobilities, i.e., hole mobility in conjugated polymers and electron mobility in fullerene derivatives, can also enhance the charge-transport efficiency of the blend film to improve the photovoltaic parameters. Thus, besides the fine-tuned electronic structure, control of solubility and crystallinity of photovoltaic materials are of extreme importance to optimize the phase separation process. Collateral methodologies such as utilization of additives[42] and thermal or solvent annealing[43] have been developed.

In response to the rapid growth in PSC devices, excellent reviews have been dedicated to the design of conjugated polymers[26-30] and fullerene derivatives[33-35] as well as morphology control of their blend films[36-39] and utilization of nanostructured materials.[44-46] In this Feature Article, rather than listing highly efficient conjugated polymers and fullerenes for PSC applications, we will concentrate on recent exploration of unique, attractive building blocks for photovoltaic polymers and fullerene derivatives. Because of the page limitations, our examples of quinoidal units, phospholes, porphyrins, and fluorinated aromatic rings as well as fullerene bisadduct regioisomers are presented together with related representative work. Furthermore, we will introduce optoelectronic devices of one-dimensional (1D) organic donor–acceptor (D–A) nanostructures that can provide the platform to examine the optoelectronic properties of organic semiconductors at nanoscale. This article is by no means a comprehensive review of PSC researches, but our emphasis

lies on how unprecedented electronic and nano-sized structures of the organic semiconductors influence their photovoltaic and photoelectric properties.

2. Conjugated Polymer Materials

To absorb the sunlight efficiently, researchers have explored low bandgap conjugated polymers. It has been shown that construction of the low bandgap polymers is attainable by the following approaches: (1) enlargement of the π systems using fused aromatic rings, (2) construction of D–A alternating backbones with an electron-rich donor and an electron-deficient acceptor units, (3) stabilization of the quinoid resonance structure, and (4) attachment of strong electron-withdrawing substituents. By using or combining these approaches, hundreds of conjugated polymers have been prepared in the last decade in pursuit of ideal materials for PSC applications.[26-30] Especially, an appropriate choice and combination of D–A units with fused ring structures enables fine-tuning of the HOMO–LUMO energy levels and their bandgaps to maximize the PCE in BHJ solar cells. Almost all of conjugated polymers for PSCs with the high PCE reported so far possess the D–A structures of fused rings based on the approaches (1) and (2).

2-1. Quinoid Polymers

2-1-1. Quinoid Homopolymers

In this section, we put emphasis on conjugated polymers based on the above-mentioned approach (3); utilization of quinoidal units. Generally, conjugated polymers are expressed in either an aromatic form with single carbon bonds or a quinoid form with double bonds between the monomer units. In most cases the aromatic form is more stable than the quinoid one, but one can stabilize the quinoid resonance form by fusing other aromatic units to the main-chain aromatic ones. Conjugated polymers with the quinoidal character would possess reduced bond length alternation and efficient

electron-delocalization along the backbone, thereby narrowing the bandgap.

One of well-known quinoidal polymers is poly(isothianaphthene) (PITN) (Fig. 2).[47,48] This polymer is of historic significance because it is the first example of "low bandgap" polymers. The ITN monomer has a bicyclic structure comprised of a phenyl ring fused to the C_3–C_4 bond of thiophene, resulting in competing aromaticity between the two rings. It has been calculated that the quinoidal form of PITN is lower in energy by 2.4 kcal mol^{-1} than the aromatic one, as a result of larger aromatic stabilization energy of benzene than thiophene.[49] This energy difference imparts significant quinoidal character to the structure of PITN, making the bandgap of PITN as low as 1.0 eV.[48] Poly(thieno[3,4-*b*]pyrazine)[50] and poly(thieno[3,4-*b*]thiophene)[51] (Fig. 2) are also known to favor the quinoid structure with narrow bandgaps of 0.95 eV and 0.8 – 0.9 eV, respectively. The major drawbacks of these homopolymers are low molecular weights, poor film-forming properties, and high-lying HOMO energy levels.[47-52] Therefore, applications of the simple homopolymers to PSC devices have not been addressed. However, engineering the substituents on these units together with a combination with other donor or acceptor units is expected to attain the excellent solubility and the lowering of the HOMO energy levels, making the quinoid-inducing units fascinating for PSC applications. In fact, Yu and coworkers have developed a series of conjugated polymers comprised of thieno[3,4-*b*]thiophene (TT) with electron-withdrawing fluorine and carbonyl substituents and electron-rich benzo[1,2-*b*:4,5-*b*']dithiophene (BDT).[53-55] These TT-based polymers have a relatively low bandgap of ca. 1.6 eV and a HOMO level of –5.2 eV. Noteworthy, this series of polymers have set the milestones of 7-9% PCEs,[12,13,20,22,53-55] and thus a number of the review articles have appeared.[28,56-59] As described below, we present a different class of the ITN-containing quinoidal D–A polymers. Namely, an intrinsic quinoidal unit such as thienoquinodimethane is applied to D–A conjugated polymers for BHJ PSCs.

Fig. 2

2-1-2. Isothianaphthene as a Donor Unit

Sariciftci and coworkers reported the PSC applications of ITN-containing polymers prepared by chemical oxidative polymerization in 2001.[60,61] Then, Frisbie and coworkers presented the first example for the synthesis of ITN-based D–A polymers and their PSC application in 2009.[62] Stille coupling reaction between 1,3-bis(trimethylstannyl)isothianaphthene[63] and bis(iodothienyl)benzothiadiazole yielded polymer **P1** (Fig. 3) with a number-average molecular weight (M_n) of 5700. The ITN-benzothiadiazole (BTD) alternating polymer **P1** showed a relatively small optical bandgap of 1.55 eV, arising from the quinoidal D–A alternating structure. A BHJ PSC device with a benchmark fullerene derivative, [6,6]-phenyl-C_{61}-butyric acid methyl ester ([60]PCBM), gave a J_{SC} of 3.4 mA cm^{-2}, a V_{OC} of 0.83 V, and a *FF* of 0.32, affording a PCE of 0.90% (Table 1) under standard AM1.5 conditions. This result demonstrated the possibility of ITN as the electron-rich unit in D–A polymers, but the PCE value was inferior to those of other BTD-based polymers.[64] The authors attributed the low PCE value to the insufficient charge mobilities.[62] One of the plausible reasons for vitiating the mobilities and resultant device performances is the instability of the ITN monomers owing to its high reactivity at the 1- and 3-positions, which would lead to the low molecular weight and considerable defect structures in the resulting polymers.

Fig. 3 and Table 1

A potential strategy to overcome the instability of the ITN monomers is the synthesis of precursor polymers from the corresponding stable monomers and the conversion of the precursors

to the desirable ITN-containing polymers by external stimuli such as heat and light after the film formation using spin-coating. Ono et al. reported the synthesis of ITN oligomers (i.e., monomer to trimer) via bicyclo[2.2.2]octadiene (BCOD)-fused thiophene, which can be converted to the ITN structure by thermally induced retro-Diels–Alder reaction.[65,66] We applied the thermal conversion method[67] to D–A alternating conjugated polymers, that is, the synthesis of novel conjugated polymers **P2** containing ITN dimer structure as a donor and thiazolothiazole unit (TT) as an acceptor in the backbone (Fig. 3).[68] Thiazolothiazole bearing two alkylthiophene units was chosen as an acceptor unit because it has strong electron-withdrawing character, rigid coplanar structure, and sufficient solubility. First, a soluble precursor polymer **P-P2** with an alternating main chain structure of BCOD-fused thiophene dimer and BDT was synthesized by palladium(0)-catalyzed Stille coupling reaction. The M_n value of **P-P2** was as high as 10000. The BCOD moiety underwent the retro-Diels–Alder reaction by the thermal treatment of a red **P-P2** film to afford a dark blue **P2** film that was insoluble in any organic solvents (Scheme 1). The optical bandgap of **P2** (1.3 eV) became significantly narrow compared to that of **P-P2** (2.1 eV) as a result of the stabilized quinoid resonance structure of the **P2** main chain.[68] The field-effect hole mobility (μ_h) of **P2** was determined to be 2.2×10^{-4} cm^2 V^{-1} s^{-1} with an on–off ratio (I_{on}/I_{off}) of 2.5×10^2, whereas the corresponding **P-P2**-based device did not show any p- and n-type response. PSC devices were fabricated based on a BHJ film of the polymers and [60]PCBM. The device with the **P2**:[60]PCBM film exhibited a PCE of 0.29% (J_{SC} = 2.41 mA cm^{-2}, V_{OC} = 0.42 V, FF = 0.29) (Table 1). The photoresponse of the **P2**:[60]PCBM-based device ranges widely from 400 nm to 900 nm in the incident photon-to-current efficiency (IPCE) spectrum, reflecting the broad absorption band of **P2**.[68] However, the device performances are still unsatisfactory. To take full advantage of the broad absorption of the low bandgap polymers containing thermally induced ITN structures for high-performance photovoltaic devices, it would be essential to optimize the molecular alignment in

the composite films with [60]PCBM, which could be modulated by altering the side-chain structures and annealing conditions.

Scheme 1

Recently, Anandan et al. developed a D–A alternating copolymer **P3** containing ITN as a donor unit and 1,4-bis-(cyano-2-thienylvinylene)phenylene as an acceptor unit by chemical oxidative polymerization (Fig. 3).[69] Despite success in obtaining the high molecular weight polymer (M_n = 398000), a PCE of the PSC device with **P3** and [60]PCBM remained moderate (1.98%, Table 1). The relatively wide bandgap (1.86 eV) and the phase separation into large domains of 30 – 110 nm resulted in the moderate J_{SC} value (4.89 mA cm^{-2}).

2-1-3. Isothianaphthene as an Acceptor Unit

In the series of TT-BDT alternating polymer with excellent photovoltaic properties,[53-55] electron-withdrawing carbonyl and fluorine have been introduced to the TT unit, rendering TT an electron deficient unit (vide infra). The electron-withdrawing substituents can also stabilize the quinoidal monomer for diminishing the instability. Inspired by these pioneering works, several groups have developed acceptor units based on ITN with electron-withdrawing groups.[70-74] Fréchet et al.[70] and Chen et al.[71] independently reported conjugated polymers **P4a** and **P4b** composed of BTD and ITN bearing two electron-withdrawing ester groups (Fig. 3). Both polymers have relatively high molecular weights (M_n > 20000) and low bandgaps (1.5 – 1.6 eV). PSCs based on these polymers as donors and [60]PCBM as acceptor exhibited PCEs of 2.74% for **P4a** and 1.25% for **P4b** (Table 1). The theoretical calculations of **P4b** suggested that a small dihedral angle between the adjacent BTD and ITN units would result in a planar conjugated backbone, leading to the higher

charge mobility and resulting higher PCE.[71] The less hindered methyl ester group in **P4a** may be responsible for the higher PCE than **P4b** with the more hindered ethyl ester.

An example of the successful acceptor unit in combination with BDT for the PSC applications is 5-alkyl-thieno[3,4-*c*]pyrrole-4,6-dione (TPD).[75-78] The optical bandgap for these systems was reported as ca. 1.8 eV, with a HOMO level of –5.4 eV and optimized PCEs exceeding 8%.[24] Noteworthy is that bandgaps of the TPD-BDT-based polymers are relatively large, suggesting room for further optimization. ITN analogues of the TPD unit, i.e., 5-alkyl-thieno[3,4-*f*]isoindole-5,7-dione (TID)[79,80] are candidates with a strong electron-accepting ability, similar to TPD, but the quinoid resonance structure is also stabilized. Three different research groups independently developed D–A alternating polymers **P5** and **P6** consisting of the BDT and TID units (Fig. 3),[70,81,82] which exhibited narrow bandgaps of 1.4 – 1.6 eV. PCE values of 2 – 3% were obtained for the PSC devices with the **P5**:[60]PCBM or **P6**:[60]PCBM layer (Table 1), which are the best performances for the ITN-based PSCs. However, despite the optimal bandgaps, the PCEs decreased compared to their TPD-containing analogues.[78] Braunecker ascribed the inferior device performance to the molecular planarity, because computational modeling suggests the TID copolymers possess a twisted backbone that is similar to polymers containing the ITN unit with two ester groups, whereas the TPD copolymers are considerably more planar and form partially ordered domains.[81] To improve the device performance, it may be necessary to build up more planar structures of ITN-based polymers, e.g., introduction of less-hindered fluorine as an electron withdrawing substituent and insertion of ethynylene bridges next to the ITN unit.

2-1-4. Thienoquinodimethane as a Donor Unit

Following the synthesis of PITN, from which low bandgap polymers are originated, poly(arylene-methine)s (PAMs) combining heteroquinodimethane and heteroaromatic units in the

main chain were prepared through the acid-catalyzed polycondensation reactions between heteroaromatic compounds and aldehydes and subsequent oxidations.[83-87] Although this approach yielded poly((oligo)thienylene-methine)s,[84] poly(ITN-methine)s,[85] and poly(pyrrolylene-methine)s[86] with a low bandgap of ca. 1.2 eV, these polymers suffered from irregularly linked heteroaromatic units and contamination of residual oxidants. In addition, the number-average molecular weights were found to be typically less than 5000. Accordingly, PAMs have yet to be applied to optical and electrical devices such as PSCs and organic field-effect transistors. Meanwhile, Jenekhe and Chen presented the synthesis of quinoid thiophene oligomers (i.e., monomer to trimer) as model compounds of PAMs.[87] These compounds exhibited efficient π-electron delocalization with absorption maxima of 480–676 nm. Moreover, the bandgap and ionization potential decreased with increasing the length of the quinoid oligomer.[87] Therefore, these electron-rich quinoidal thiophene units can be regarded as highly promising building blocks for D–A conjugated polymers with a tunable bandgap and HOMO level.

Recently, we synthesized a non-fused ring building block of an electron-rich quinoid structure, 2,5-thienoquinodimethane to incorporate it into D–A type low bandgap polymers for the first time.[88] Specifically, 2,5-thienoquinodimethane **P7a** and **P7b** with 4-(*tert*-butyl)phenyl or 4-(octyloxy)phenyl side chain as a solubilizing group was copolymerized with an electron-deficient diketopyrrolopyrrole (DPP) subunit (Fig. 3). Note here that we used mixtures of *E,E*, *E,Z*, *Z,Z* isomers of the thienoquinodimethane monomers due to the difficulty in separation. The obtained polymer films exhibited broad and intense absorption bands in the region of 400–1000 nm. Photovoltaic devices with active layers consisting of **P7a** or **P7b** with [6,6]-phenyl-C_{71}-butyric acid methyl ester ([70]PCBM) revealed a broad photoresponse covering from 400 nm to 1000 nm. In contrast, the PCE values were found to be moderate (PCE = 1.44%, J_{SC} = 6.58 mA cm^{-2}, V_{OC} = 0.53 V, and *FF* = 0.42 for **P7a**; PCE = 0.96%, J_{SC} = 5.58 mA cm^{-2}, V_{OC} = 0.45 V, and *FF* = 0.41 for **P7b**,

Table 1) under the illumination of AM1.5G, 100 mW cm^{-2}.[88] The V_{OC} values are inferior to those of the devices consisting of other DPP-based conjugated polymers,[89] reflecting the shallow HOMO levels (–5.2 eV for **P7a** and –4.9 eV for **P7b**) because of the strong electron-donating character of the 2,5-thienoquinodimethane units. The superior PCE value of the **P7a**:[70]PCBM-based device relative to the **P7b**:[70]PCBM-based one can be rationalized by the more favorable phase-separated nanostructure in the active layer as well as the higher crystallinity of **P7a** than **P7b**. Although these PCE values are lower than those on the state-of-the-art PSC devices, these results corroborate the "true" quinoid structures can function as a building block of D-A conjugated polymers. This approach is versatile for the creation of novel low bandgap polymers as well as the utilization of the fused-ring structures.

2-2. Phosphole Polymer

Despite the diversity of elements in the periodic table, majority of conjugated polymers for PSC applications are characterized by the backbones that only contain carbon in combination with sulfur, nitrogen, and oxygen. Under such circumstance, a material design approach that has generated much attention in recent years is the incorporation of other heteroatoms in the polymer backbone. Non-fused and fused heterocycles partially substituted with larger heteroatoms such as silicon, germanium, and selenium are anticipated to have several advantages over conventional monomer units composed of C, S, N, and O. For instance, the reduced aromaticity of selenophene, compared to thiophene, increases the ground-state quinoid resonance character of its polymers, resulting in improved planarity, increased effective conjugation length, and facilitated interchain charge hopping.[90,91] Besides, conjugated polymers containing bithiophene systems fused by Si and Ge showed enhanced solid-state ordering and also improved charge transport in comparison with the carbon-fused analogues.[92,93] Therefore, these polymers revealed, albeit not always,[94] higher PCE

values than the thiophene or carbon-fused counterparts.

Among the various heterocycles, phosphole has a unique feature; the LUMO level is influenced by hyperconjugative interactions, and can be lowered significantly by variation of the phosphorus substituent.[95] In this regard, thiophene–phosphole-based D–A-type copolymers, in which the phosphole acts as an acceptor unit, are attractive low bandgap conjugated polymers for the use in PSCs. To date, several kinds of phosphole-containing π-conjugated polymers have been reported,[96-99] but they had never been applied to PSC active layers. Recently, we have reported the first example of thiophene–phosphole-based D–A-type copolymers for BHJ PSCs.[100] Namely, two kinds of phosphole- and BDT-based copolymers **P8a** and **P8b** bearing P^V=O and P^V=$NSO_2C_8H_{17}$, respectively, were prepared by Pd–CuI-promoted Stille coupling reactions (Fig. 4). The optical HOMO–LUMO gaps of **P8a** and **P8b** determined from their absorption onsets in films were found to be 1.73 and 1.69 eV, respectively. The HOMO levels obtained by photoemission yield spectroscopy were –5.65 for **P8a** and –5.32 eV for **P8b**, which are lower than those of the TT and BDT-based polymers (ca. –5.2 eV).[53-55] These results suggested that the incorporation of the phosphole subunits is effective for lowering the HOMO levels of the D–A copolymers. On the other hand, PSC device performances differed significantly depending on the P=E functions (E = O, $NSO_2C_8H_{17}$).[100] The device with the **P8b**:[70]PCBM active layer showed a higher PCE of 0.65% (J_{SC} = 2.6 mA cm^{-2}, V_{OC} = 0.63 V, *FF* = 0.40) than that with **P8a**:[70]PCBM (PCE = 0.07%, J_{SC} = 0.45 mA cm^{-2}, V_{OC} = 0.45 V, *FF* = 0.35). Presumably, the **P8b** π network is more densely packed and transports the charge carriers more effectively than the **P8a** π network owing to the less steric congestion around the phosphorus core of **P8b**. This implies that the P^V substituents make a large impact on the charge-generation efficiency and/or charge-carrier transports in the blend films. The preliminary PCE value of 0.65% as well as the other photovoltaic parameters is still low compared to the previously reported PCE values for PSC devices with BDT-based D–A copolymers.[26-30]

Nevertheless, these results exemplify for the first time that the phosphole subunits can behave as key components in the D–A copolymers for PSC.

Fig. 4

2-3. Porphyrin Polymer

In a quest for monomer units that may provide major PCE breakthroughs, the utilization of highly light-absorbing chromophore units with unique optical and electronic properties is also an enchanting approach. Among various chromophores, porphyrins and their derivatives have attracted considerable attention for many years, preliminarily because of their importance in biological systems.[101] In most of natural photosynthetic cores of plants, solar energy is absorbed by chromophores based on porphyrin framework and the absorbed solar energy is converted efficiently to chemical energy. Porphyrins consist of an extensively conjugated planar π-system which renders them suitable for light-harvesting and efficient ET because the uptake or release of electrons results in minimal structural change.[102] Typical porphyrins exhibit an extensive optical absorption in the visible region, i.e., intense Soret band at 410 – 430 nm and moderate Q bands at 500 – 650 nm. Their electrochemical and photophysical properties can be tuned easily via synthetic modifications at the macrocycle peripheral positions and by metal insertion into the central cavity. These remarkable physical and chemical properties make porphyrins suitable for light-absorbing dyes in dye-sensitized solar cells (DSCs).[103-105] In fact, porphyrins have been proven to be one of the most promising materials for highly efficient DSCs yielding a record PCE of 12.3% for DSCs.[103] In view of these captivating properties, porphyrin frameworks have also been employed in PSC devices.[106-113]

The first example of the synthesis and PSC applications of conjugated polymers with porphyrins

as a unit of the main chain was reported by Bo and coworkers in 2008.[106] Soluble conjugated alternating porphyrin-dithienothiophene copolymers **P9a** and **P9b** with direct and triple-bond linkage (Fig. 5) were synthesized by palladium(0)-catalyzed Stille and Sonagashira coupling reactions, respectively. It is noteworthy that both porphyrin and dithienothiophene units in the polymer main chain are electron-rich donor monomer units, and thus **P9a** and **P9b** are not D–A alternating copolymers. The absorption spectrum of **P9a** in thin film exhibits a sharp Soret band at 450 nm and two weak Q-bands at 560–620 nm, while **P9b** does a sharp Soret band at 491 nm and a strong Q-band at 760 nm. In polymer **P9b**, the triple-bond linker between the porphyrin and dithienothiophene units reduces the steric hindrance and, therefore, may promote coplanarity and extended π-conjugation. Consistently, the PSC device with the **P9b**:[60]PCBM active layer showed a higher J_{SC} (1.52 mA cm^{-2}) and thereby enhanced the photovoltaic parameters (PCE = 0.30%, V_{OC} = 0.58 V, FF = 0.34) compared to those with **P9b**:[60]PCBM (J_{SC} = 0.45 mA cm^{-2}, PCE = 0.06%, V_{OC} = 0.45 V, FF = 0.29) under the same condition.[106]

Fig. 5

On the other hand, we investigated the effects of the heterole bridges (i.e., furan vs. thiophene) in porphyrin polymers on their PSC performances as well as optical, electrochemical, and photophysical properties.[107] Conjugated polymers **P10a** and **P10b** with alternating main chain structures of zinc porphyrin-furan and zinc porphyrin-thiophene were synthesized by Stille coupling reaction (Fig. 5). The optical bandgap of 1.75 eV for **P10a** is smaller than that of 1.90 eV for **P10b**, implying the efficient delocalization of the π-electrons along the polymer main chain of **P10a** relative to **P10b**. The more extended π-conjugation in **P10a** originates from the smaller steric repulsion of the *meso*-furan moiety with the porphyrin rings than that of the *meso*-thiophene. In

fact, dihedral angles between the porphyrin and furan or thiophene were estimated to be 43° for **P10a** and 70° for **P10b** by theoretical estimation. The time-resolved fluorescence spectrum of **P10a** showed a gradual Stokes shift to the longer wavelength in the subnanosecond time domain due to the relaxation from a twisted conformation with the large dihedral angles between the porphyrins and the furan rings to a coplanar conformation with the small dihedral angles, whereas the fluorescence spectrum of **P10b** did not exhibit such dynamic Stokes shift. Both **P10a** and **P10b** are electrochemically active in the oxidation and reduction regions and have suitable HOMO and LUMO levels that enable photoinduced ET from the excited state of the polymer to [60]PCBM in the blend films. Indeed, the blend films displayed strong fluorescence quenching of the porphyrin moieties by [60]PCBM together with appearance of charge-transfer (CT) emission arising from the interaction between the porphyrin and the C_{60} moieties. This is the first observation on CT emission between conjugated porphyrin polymers and fullerenes. PSCs were fabricated by using the blend films of **P10a**:[60]PCBM and **P10b**:[60]PCBM as photoactive layers.[107] The **P10a**:[60]PCBM and **P10b**:[60]PCBM devices revealed PCEs of 0.048% and 0.027% under standard AM1.5 sunlight (100 mW cm^{-2}). Unfortunately, formation of the supramolecular CT complexes arising from the conjugated porphyrin polymer and fullerene does not enhance the device performance of the BHJ PSCs probably due to the lack of bicontinuous polymer-fullerene network in the photoactive layer. Nevertheless, these results obtained in this study will provide fundamental information on the rational design of large chromophore-embedded conjugated polymers for solar energy conversion.

After the above two pioneering works, several groups synthesized porphyrin conjugated polymers and applied them to active layers in PSCs. Zhou et al. incorporated an acceptor unit, i.e., BTD, into porphyrin polymers.[110] Namely, conjugated polymers containing the porphyrin, thiophene, and BTD units were synthesized by Stille coupling reaction of 2,5-bis(trimethylstannyl)thiophene with BTD and porphyrin bearing bis(bromoaryl) groups (**P11a**

with x : y = 1 : 2 and **P11b** with x : y = 1 : 4, Fig. 5). With increasing the molar amount of BTD moieties in conjugated main chain, the absorption in the range of 450–700 nm was broadened and red-shifted compared to the similar polymers without the BTD moiety, and the optical bandgaps of copolymers were narrowed to ca. 1.50 eV. The PSC device fabricated based on the **P11b**:[60]PCBM film showed a PCE of 0.91%. Although the PCE was improved by the incorporation of D–A structures relative to the preceding works, it is far from bringing out the full potential of porphyrins in PSCs. The large drop of absorption between the Soret and Q bands as well as less efficient conjugation length in the main chain owing to the large dihedral angles between the porphyrin and adjacent aryl group is responsible for the limitation in the photovoltaic properties.[106-111] To avoid the large porphyrin–aryl dihedral angles in porphyrin polymers with *meso*-linkage, Wang and coworkers recently proposed an edge-fused fashion to form quinoxalino[2,3-*b*]porphyrin (QP) moiety as a new acceptor unit.[112,113] They prepared a ternary copolymer **P12** composed of terthiophene with QP and carbazole units (Fig. 5). **P12** displayed a broad absorption over the entire spectrum of visible light without a missing absorption region between Soret and Q bands, which is beneficial for enhancing its light-harvesting ability. The dihedral angles between the π bridge and QP were estimated to be ca. 20° by a theoretical calculation, which are in good agreement with the larger π extension in **P12** obtained by the absorption measurements. The PSC fabricated from the blend of **P12** and [70]PCBM showed a PCE value as high as 2.53% with a V_{OC} of 0.68 V, a J_{SC} of 8.32 mA cm^{-2} and a *FF* of 0.45. This result indicates that porphyrin-acceptor alternating structures could be promising as D-A units of conjugated polymer for highly efficient PSCs.

2-4. Fluorinated Polymer

Another potential approach to broadening of the absorption bands and downward-shift of the

HOMO and LUMO energy levels of D–A conjugated polymers is the attachment of electron-withdrawing groups to the monomer units (vide supra). In the electron-withdrawing substituents, fluorine atom substitution, as the smallest electron-withdrawing group in size, is ideal in downward-tuning of the HOMO and LUMO energy levels without disturbing the planar molecular structure. In particular, the D–A copolymers consisting of electron-donating BDT and fluorine-substituted TT with a carbonyl group, i.e., PTB7, revealed leading PCE values of single-junction PSCs.[12,13,20,22,53-55] Inspired by these successful works, Zhou et al. first reported the synthesis of a conjugated polymer with an incorporated fluorinated BTD unit, and demonstrated its improved performance relative to the unsubstituted BTD moiety in the PSC.[114] The increase in the device performance arose predominately from a deeper HOMO level which increased the V_{OC} value of the PSC. They and others have subsequently reported the use of the mono- and di-fluorinated BTD unit[23,115,116] as well as fluorinated quinoxaline,[21,117] 2-alkyl-benzo[*d*][1,2,3]triazole,[118] and vinylene,[119] which in general resulted in an improved photovoltaic performance.

Along with PTB7, poly[*N*-9'-heptadecanyl-2,7-carbazole-*alt*-5,5-(4',7'-di-2-thienyl-2',1',3'-benzothiadiazole)] (PCDTBT, Fig. 6) is now a benchmark polymer that shows a relatively low HOMO level (–5.5 eV) and excellent photovoltaic performances in PSCs.[120-122] PCDTBT is stable and low-cost materials for PSCs with a high V_{OC} of 0.90 V, a PCE of 7.5%, and an estimated lifetime of 7 years.[122] However, the bandgap of PCDTBT (1.89 eV) is larger than the value (1.5 – 1.7 eV) of the ideal polymers for the PCE exceeding 10%. Recently, to narrow the bandgap of PCDTBT without sacrificing the low HOMO level, further different electron-accepting monomers, including phenylbenzotriazole[123] and quinoxaline-based units,[124] have been incorporated into 2,7-carbazole based copolymers. However, the PCE values of the PSCs with these polymers are still comparable to or even lower than those of the PCDTBT-based devices.

To shed light onto the effect of fluorine substitution on the photovoltaic properties of PCDTBT

as well as its molecular and film structures and optical and electrochemical properties, we recently combine 4,7-di(thien-2-yl)-5,6-difluoro-2,1,3-benzothiadiazole (DTBT-F) with carbazole for the first time to obtain a fluorinated analogue of PCDTBT (**P13**) where two hydrogen atoms on the BTD units are replaced by two fluorine atoms (Fig. 6).[125] In addition, **P14** with additional hexylthiophenes between the thiophene and carbazole of **P13** was also prepared to overcome the poor solubility of **P13** (Fig. 6).[125] The **P14** film showed wide absorption in UV and visible regions with an optical bandgap of 1.82 eV that is smaller than that of PCDTBT, whereas the film of **P13** exhibited blue-shifted absorption with a bandgap of 1.96 eV due to the low molecular weight (M_n = 4000) arising from the deficient solubility. The HOMO energy level of **P13** was successfully lowered by the fluorination of BTD unit (–5.54 eV), whereas **P14** exhibited a higher HOMO level (–5.44 eV) than PCDTBT (–5.48 eV), implying that the additional incorporation of electron-donating hexylthiophenes negated the fluorination effect. PSC devices that employed **P13** or **P14** as an electron donor and a fullerene derivative [70]PCBM as an electron acceptor yielded lower PCEs of 1.29% (V_{OC} = 0.82 V, J_{SC} = 4.93 mA cm^{-2}, *FF* = 0.32) and 1.98% (V_{OC} = 0.88 V, J_{SC} = 6.56 mA cm^{-2}, *FF* = 0.34) than that (6.16%) of PCDTBT (V_{OC} = 0.88 V, J_{SC} = 11.1 mA cm^{-2}, *FF* = 0.63). Unfavorable film structures, low crystallinities, and limited exciton lifetimes of the fluorinated polymers are responsible for the decrease in the PCE.[125] Considering the availabilities of fluorinated analogues of PCDTBT to lower the HOMO energy levels, there is still room to achieve higher PCEs in the BHJ PSCs. To take full advantage of the lower HOMO level of the fluorinated PCDTBT analogues for high-performance photovoltaic devices, it would be desirable to optimize the molecular alignment in the films, which could be modulated by altering the side-chain and end-group structures and utilizing additives.[24,42,126-128]

Fig. 6

3. Fullerene Materials

As already described above,[16,17] it is well established that the magnitude of V_{OC} value is proportional to the difference between the HOMO level of the donor and the LUMO level of the acceptor. At the molecular level, lowering the HOMO level of conjugated polymers or raising the LUMO level of fullerene derivatives or the both could reach the larger V_{OC} value. However, lowering a polymer's HOMO level inevitably increases its optical bandgap and thereby sacrifices its light-harvesting ability. Meanwhile, trimetallic nitride endohedral fullerenes (TNEFs) are known to possess up-shifted LUMO levels compared to their corresponding empty-cage fullerenes.[129] In 2009, Ross et al. synthesized a soluble PCBM-like $Lu_3N@C_{80}$ derivative with hexyl chain (Lu_3N@[80]PCBH).[130] The LUMO level of Lu_3N@[80]PCBH is 0.28 eV higher than that of [60]PCBM. When comparing the photovoltaic properties of poly(3-hexylthiophene) (P3HT):Lu_3N@[80]PCBH- and P3HT:[60]PCBM-based devices, J_{SC} and *FF* were similar but V_{OC} of the former was 0.26 V higher than that of the latter. Thus, the endohedral fullerenes can be excellent acceptors attaining high V_{OC} in PSC. However, the high production and separation costs as well as the low reactivity of the endohedral fullerenes still hamper their wide application in PSC devices.

It has also been reported that fullerene bis- and multi-adducts of fullerenes effectively enhance the V_{OC} values by 0.1 – 0.2 V compared to the corresponding mono-adducts.[131] The second functionalization on the fullerene framework of the mono-adduct further reduces the π-conjugation as well as electron delocalization in the fullerene. This structural alternation in the bis-adduct makes the first one-electron reduction potential more negative, thereby yielding the higher-lying LUMO level. Successful examples such as PCBM bisadduct (bis-PCBM),[132] indene-C_{60} and -C_{70} bisadduct ([60]ICBA and [70]ICBA),[133,134] di(4-methylphenyl)-methano-C_{60} bisadduct (DMPCBA),[135] and thieno-*o*-quinodimethane-C_{60} bisadduct (TOQC)[136] have been reported. In particular, a combination

of [70]ICBA with P3HT achieved a PCE as high as 7.5%.[134] Despite successful application of fullerene bisadducts to PSCs, their regioisomer mixtures have been directly used without separating each isomer. Considering that molecular packing and arrangement of fullerene derivatives in the active layer with polymers have a large impact on CS and electron-transporting properties, a pure bis- or multi-adduct isomer with the multi-substituents at specific positions on C_{60} would yield a more desirable network structure in the BHJ active layers by the excellent matching of the polymer and each multi-adduct isomer. Overall, a better photovoltaic performance in a specific combination of the polymer and pure fullerene bis- or multi-adduct isomer is expected, compared to the corresponding combination of the polymer and fullerene bis- or multi-adduct mixtures. Accordingly, it is extremely important to elucidate the close relationship between the molecular structure of fullerene bis- or multi-adduct regioisomers and photovoltaic performance.

Nakamura and coworkers reported the regiocontrolled synthesis and photovoltaic application of a new class of structurally defined 66π-electron tetra-organo[70]fullerenes.[137] Namely, they developed a synthetic access to [3+1] hybrid tetra-aryl C_{70} adducts via oxidation of a fullerene copper complex $[Ar_3C_{70}\text{-Cu-Ar'}]^-$ (Ar = 4-*n*BuC_6H_4, Ar' = 4-MeOC_6H_4). This reaction yielded only two types of regioisomers (Fig. 7), 3,10,22,25-adduct **F1** and 7,10,22,25-adduct **F2**. The generation of the two regioisomers was suggested to result from the haptotropic migration of the copper on a cuprio fullerene intermediate. **F1** was easily separated by gel permeation chromatography (GPC) and residual **F1** in the mixture with **F2** was thermally converted to **F2**, yielding both pure **F1** and **F2**. Although **F1** and **F2** bear the same substituents on the surface of C_{70}, the difference in the first reduction potentials is notable, that is, the LUMO level of **F1** (–3.72 eV) is lower by 0.1 eV than that of **F2** (–3.62 eV). In addition, organic photovoltaic (OPV) devices having a bilayer active layer of tetrabenzoporphyrin (BP) as an electron donor and **F1** or **F2** as an electron acceptor were fabricated with a configuration of ITO/PEDOT:PSS/BP/**F1** or **F2**/NBphen/Al (NBphen:

2,9-bis(naphthalen-2-yl)-4,7-diphenyl-1,10-phenanthroline).[137] As expected from the LUMO levels, the device with **F2** showed a higher V_{OC} of 0.87 V than that of the device based on **F1** (0.74 V), and the corresponding higher PCE of 2.87% than that of 1.18%. In accordance with the PCEs, the **F2** regioisomer revealed a J_{SC} of 5.52 mA cm^{-2} and a *FF* of 0.60, whereas the **F1** regioisomer a J_{SC} of 3.66 mA cm^{-2} and a *FF* of 0.44. J_{SC} and *FF* values are known to correlate with the carrier mobility of the materials[18,19] and close packing of the fullerene cores in the blend film is the key factor for effective electron hopping in the OPV devices. Thus, the higher performance of the **F2**-based OPV device can be attributed at least partially to the higher electron mobility of the **F2**-based blend film. This can be rationalized by a closer fullerene-fullerene distance in the crystals of **F2**, as compared to **F1**. These findings corroborate the necessity of developing selective synthesis or facile separation methodology of fullerene regioisomers for the rational design of organic semiconductor materials.

Fig. 7

Aside from the above notable exception,[137] the current synthetic routes to fullerene bis- and multi-adducts invariably generate a mixture of regioisomers.[132-136] Therefore, we recently conducted the separation of C_{60} bisadduct regioisomers **F3** (Fig. 8) and applied the separated bisadducts to PSCs for the first time.[138] To reduce the number of fullerene bisadduct isomers, a symmetrical dihydronaphthyl group was chosen as the substituent. We expected that symmetrical introduction of two long alkoxycarbonyl chains into the dihydronaphthyl groups would facilitate the isomer separation and purification. To our satisfaction, repeated separations by HPLC equipped with a Buckyprep column afforded *trans*-1, *trans*-2, *trans*-3, *trans*-4, *e*, and *cis*-2+*cis*-3 (mixture) isomers, named by Hirsch nomenclature,[139] with a ratio of 3 : 18 : 31 : 11 : 29 : 7 (Fig. 8). *cis*-1 isomer could not be obtained because of steric hindrance. The LUMO energy levels of the **F3** isomers estimated

by cyclic voltammetry are 0.1 – 0.2 eV higher than those of the monoadduct **F4** and [60]PCBM (Table 2), which would be favorable for their application as an acceptor in PSCs to improve V_{OC}. PSCs based on P3HT:**F3** or P3HT:**F4** without a cathode buffer layer were fabricated and the device performances were evaluated under standard AM1.5 conditions (Table 2).[138] The *trans*-2, *trans*-4 and *e* isomer-based PSCs exhibited comparable PCE values of ca. 1.4%, whereas the *trans*-1, *trans*-3 and *cis*-2+*cis*-3 isomer-based BHJ solar cells revealed significantly inferior performance (PCE = 0.12-0.89%). Overall, the regioisomer mixture (**F3** mixture)-based device showed moderate performance (PCE = 0.95%). Although the PCE (1.71%) value of the **F4**-based device is slightly higher than those of *trans*-2, *trans*-4 and *e* isomer-based devices, the V_{OC} values (0.70–0.73 V) of the bisadduct-based devices are significantly increased compared to that (0.66 V) of the monoadduct-based device. The IPCE values of the *trans*-2-based device are larger than those of the *trans*-3-based one, despite of similar light-harvesting properties of the two films.[138] This indicates that the difference in the device performance results from those in CS efficiency and/or charge-collection efficiency. Consistently, the surface morphology of the P3HT:**F3** (*trans*-3) film showed micrometer-sized phase separation, whereas the P3HT:**F3** (*trans*-2) film did not show such large aggregations. These results suggest that a bicontinuous D−A network is formed more effectively in the P3HT:**F3** (*trans*-2) film than in the P3HT:**F3** (*trans*-3) film, leading to the higher device performance of the P3HT:**F3** (*trans*-2) device.

Fig. 8 and Table 2

Following our pioneering experimental study, Sabirov revealed the correlation between anisotropy of polarizability and photovoltaic performances based on the theoretical calculation and our experimental results.[140] The superior photovoltaic isomers, i.e., *trans*-2, *trans*-4 and *e* isomers,

are characterized by the low anisotropy, whereas the inferior photovoltaic isomers, i.e., *trans*-1 and *trans*-3, showed the high anisotropy. Such structure–photovoltaic performance relationship will provide valuable, basic information on the rational design of fullerene bisadducts as an acceptor for highly efficient PSCs.

Recently, Li et al. reported the isolation and photovoltaic performance of dihydronaphthyl-based fullerene bisadduct **F5** where no substituents are present on the benzene ring (Fig. 8).[141,142] In contrast to our study, only *trans*-2, *trans*-3, *trans*-4 and *e* isomers were isolated by HPLC. Despite the small steric hindrance owing to the absence of substituents at hydronaphthyl groups, *cis*-1, *cis*-2 and *cis*-3 isomers of **F5** where both substituents are present on the same hemisphere of the fullerene cage, were found to be low in yield. The *trans*-1 isomer of **F5** was also unavailable due to the energetic unfavorable reactivity on this site. The four **F5** isomers exhibited different LUMO levels (–3.70 ~ –3.76 eV) and electron mobility, leading to different PCE values ranging from 5.5 to 6.3% (Table 2). Overall, PCEs of the P3HT:**F5** isomer-based devices with Ca cathode buffer layer were higher than those of the P3HT:**F3** isomer-based devices, probably due to the ill-packed structure of **F3** as well as the absence of cathode buffer layer.[138] Namely, ester groups on hydronaphthyl groups of **F3** may limit the dense packing of the fullerene moieties in the blend film, although the solubilizing groups permit the isolation of *cis*-isomers and *trans*-1. Among the isomers of **F5**, the P3HT:**F5** (*trans*-3)-based PSC afforded the highest PCE value of 6.3%, which is obviously superior to the **F5** mixture based PSC (5.3%).[142] The performance improvements should be ascribed to higher LUMO energy level and higher electron mobility of the *trans*-3 **F5** isomer, suggesting the necessity to use the individual fullerene bisadduct isomer for high performance PSCs. Moreover, the electron mobility of the isomers may be related to the packing ability of the fullerene cage in the blend film. These findings imply that the two substituent positions of the fullerene bisadduct do have a pronounced effect on overall photovoltaic performance.

4. Nanostructured Devices

The advances in PCEs of PSCs have largely been achieved by the extensive synthetic efforts for new conjugated polymers and fullerene derivatives and their device evaluation, as discussed above. However, at present, our ability to predict device performances from material structures is still limited. As a consequence, the vast majority of new materials tested so far have showed inferior performance to the ongoing state-of-the-art materials such as PTB7 and PCDTBT, contrary to the prediction by the HOMO and LUMO levels. The understanding of the fundamental processes of exciton dissociation and charge transport in the polymer-fullerene films with nanoscaled BHJ structure and charge collection at organic-inorganic interfaces remains great challenges toward achieving the improvement in PCE values.

Optoelectronic devices of 1D organic nanostructures may serve as the ideal model systems to examine the optoelectronic processes of organic semiconductors at nanoscale. In fact, p-n heterojunctions of inorganic and inorganic-organic hybrid materials with 1D nanostructures offer several significant advantages not available in other material systems.[143,144] For example, they can simultaneously allow efficient optical absorption and charge transportation due to the confinement in two lateral dimension and unconstrained axial dimension. In addition, the unique geometry permits low optical reflection. These encouraging properties of inorganic and hybrid p-n junction nanostructures suggest similar advantages of pure organic p-n (i.e., D–A) junction with nano-sized 1D structures for both fundamental research and practical applications. However, reports on 1D organic D–A heterojunction are extremely limited. One reason is the difficulty of fabrication; i.e., the techniques for the fabrication of inorganic p-n junctions, such as oxidation, diffusion of dopants, and ion implantation, which are not applicable to organic semiconductors. In this section, we highlight recent efforts for the construction of organic D–A heterojunction with one-dimensionally

confined structures and their applications in photovoltaic and optoelectric devices.[145-147]

Briseno and coworkers reported the formation of single-crystalline D–A heterojunction nanoribbons of organic semiconductors by selective crystallization of copper hexadecafluorophthalocyanine acceptor F_{16}CuPc on copper phthalocyanine donor CuPc single-crystalline nanoribbons (Fig. 9).[145] The crystallization of F_{16}CuPc onto CuPc requires several parameters, including similar molecular structures and lattice constants as well as π-stacking along the nanoribbon axis. The width of the CuPc nanoribbons prepared by physical vapor deposition (PVD) technique ranged from several tens to several hundred nanometers, the thickness of several nanometers and the length from 20 to 50 μm. The length of the D–A heterojunction depended on the length of the CuPc template and the PVD crystallization time of F_{16}CuPc on the CuPc template. Ambipolar transport of the D–A heterojunction nanoribbons was observed in field-effect transistors (FETs) with balanced electron and hole mobilities of 0.05 and 0.07 $cm^2\ V^{-1}\ s^{-1}$ for F_{16}CuPc and CuPc, respectively. A photovoltaic device with the composition of Au/CuPc/F_{16}CuPc/Al (Fig. 9) was fabricated and yielded a PCE of 0.007% (J_{SC} = 0.054 mA cm^{-2}, V_{OC} = 0.35 V, FF = 0.36) under AM 1.5 simulated light, but the detailed measurement conditions (e.g., the sizes of cell and mask) were not described in the report.[145] Although the device showed the low PCE, the discrete D–A heterojunction devices may allow precise control and characterization of the optoelectronic properties, thus significantly reducing the uncertainty in data interpretation in comparison with polycrystalline bilayer devices.

Fig. 9

Recently, our group reported the first example of D–A double-cable copolymer nanorods synthesized by electrochemical copolymerization.[146] Ordered anodic aluminum oxide (AAO)

templates (Scheme 2) were used as the nano-sized templates and 3-hexylthiophene (3HT) and C_{60} were chosen as the electron donor and acceptor, respectively. To fabricate a BHJ nanorod composed of 3HT and fullerene, we synthesized thiophene-tethered C_{60} (TC_{60}) and conducted copolymerization of TC_{60} with 3HT to obtain the copolymer P(3HT+TC_{60}), where fullerenes were covalently incorporated into the polythiophene (Scheme 3). As illustrated in Scheme 2, segmented metal–polymer–metal nanorods (denoted as Au/P(3HT+TC_{60})/Au) were synthesized by 1) electrochemical deposition of gold into an AAO template, 2) electrochemical copolymerization of 3HT and TC_{60} with a molar ratio of 4:1, i.e., weight ratio of thiophene:C_{60} unit ≈ 1:1, 3) electrochemical deposition of gold, and 4) removal of the template. The incorporation of Au segments at both sides were expected to create excellent electrical connections between the P(3HT+TC_{60}) segments and Au microelectrode. SEM measurements revealed that the Au/P(3HT+TC_{60})/Au nanorods have an average diameter of 330 nm (±10 nm) with a total length of 2.7 μm (±0.4 μm) and possess distinct interfaces between the Au and P(3HT+TC_{60}) segments.

Schemes 2 and 3

The photoelectric measurements of Au/P(3HT+TC_{60})/Au nanorod revealed highly insulating nature in the dark with resistivity of 1.2×10^5 Ω·cm.[146] However when illuminated, the Au/P(3HT+TC_{60})/Au nanorod served as a semiconductor with a resistivity of 8.4×10^3 Ω·cm. In contrast, the reference Au/P3HT/Au nanorods are highly insulating both in the dark (1.6×10^5 Ω·cm) and under illumination (1.2×10^5 Ω·cm). The Au/P(3HT+TC_{60})/Au nanorod caused CS within the P(3HT+TC_{60}) segment by illumination and the generated charges were transported to the Au segments by inter- and intramolecular electron hopping through the neighboring C_{60} moieties in the BHJ nanorod. On the other hand, the Au/P(3HT+TC_{60})/Au nanorods did not show FET

properties.[146] The hole transport may be hindered by the inefficient conjugation of P(3HT+TC_{60}) owing to the bulkiness of TC_{60}. In addition, no occurrence of electron transport was caused by the large electron-injection barrier from Au (5.1 eV work function) to C_{60} (4.0 eV LUMO) as well as a significant amount of electron traps (OH, etc.) on the SiO_2 surface. Although such preliminary devices need further optimization, these systems based on organic D–A heterojunction nanorods will be useful for probing photoinduced CS and transport at nanointerfaces and in exploring the rational design of nanoscaled organic electronics including OPVs and FETs.

Subsequently, well-defined nanotubes of regioregular P3HT and [60]PCBM were reported by Hu and coworkers.[148] The P3HT:[60]PCBM BHJ nanotubes were also prepared with AAO templates, but not by the electrochemical polymerization. In their method, the AAO template was immersed into a P3HT/[60]PCBM (1:1, wt. %) solution in chlorobenzene for 48 h so that the mixed solution had sufficient time to entirely penetrate into the AAO nanopores. After the solvent evaporation, well-defined P3HT:[60]PCBM BHJ nanotubes were obtained, and the AAO template was removed. The average diameter and thickness of the nanotubes were around 200 and 30 nm, respectively. The photovoltaic devices based on individual nanotube were constructed with asymmetrical electrodes fabricated by a modified organic ribbon mask method,[149] namely Au/P3HT:[60]PCBM/Al configuration. The significant photovoltaic effect was observed under 5.51 mW cm^{-2} white light illumination. A PCE of 0.106% with J_{SC} = 0.049 mA cm^{-2}, V_{OC} = 0.47 V, and FF = 0.25 was obtained for the device where the active area was calculated by the entire length (ca. 2 μm) of conducting channel between the electrodes multiplying the width of nanotube (ca. 200 nm). The PCE value was one order higher than that of individual single crystal of planar D–A heterojunction nanoribbons (0.007%)[145] due to the BHJ structure. These works will open the door to opportunities for exploring the fabrication of nano-sized BHJ structures of organic semiconductors and their application to fundamental science as well as new nano-sized device technologies.

5. Summary and Outlook

This Feature Article has focused on recent notable design concepts to unique, attractive building blocks for conjugated polymers as electron donors as well as recent progress in separated fullerene bisadduct regioisomers as electron acceptors. In addition, we overviewed recent attempts for the construction of organic D–A heterojunction with one-dimensionally confined structures and their applications to photovoltaic and optoelectric devices. The topics in this article are not a comprehensive list of PSC researches, but involve exploration of fundamental materials and concepts to inspire further studies in PSCs.

The field of PSCs has continued to evolve, and this technology has been transferring from research laboratories to industrial massive fabrications. The PCE of the PSCs with a cell size of ca. 0.1-1 cm^2 has been steadily increased from ca. 1% in 1995[150] to recently over 9%[12] in single cells and over 10%[14] in tandem cells. However, the PCE values are always much lower than ideal. Janssen and Nelson recently proposed that PCEs of 20 – 24% are reachable in single junction PSCs with the assumption that fill factor and internal quantum efficiency are 0.85 and unity.[151] Therefore, there is still plenty of room for further improvement in the PCE values of PSCs. The suppression of charge recombination as well as the enhancement of charge dissociation at the D–A interface is pivotal in achieving the excellent device performances.[152-154] The formation of weakly bound interfacial CT states makes it possible to shut off the recombination and non-radiative deactivation.[155] The separation distance between electron-donating polymers and electron-accepting fullerenes is one of the decisive factors to control the charge recombination process. Systematic studies for revealing the effect of D–A electronic coupling in bulk heterojunction films on photodynamics and photovoltaic properties will provide valuable information for the improvement of device performance. Developments of unprecedented main-chain and side-chain structures of

conjugated polymers can also tune the interaction at D–A interfaces. Furthermore, the utilization of nano-sized organic materials such as nanorods with limited space for CS and charge dissociation may simplify the investigation of photophysical processes in PSC devices. If such structure–photovoltaic property correlation is available, this will greatly aid toward the realization of over 12% efficiency. The rational molecular design and elaborated synthesis of the photovoltaic materials will continue to play a core role for understanding the device mechanism and promoting the commercial application of PSCs.

Acknowledgements

This work is supported by New Energy and Industrial Technology Development Organization (NEDO). Authors thank Dr. Osamu Yoshikawa, Prof. Takashi Sagawa, Prof. Susumu Yoshikawa, Dr. Tatsuya Fukushima, Prof. Hironori Kaji (Kyoto University), and Prof. Akihiko Fujii (Osaka University) for the instruction of PSC device fabrication, and Prof. Yoshihiro Matano (Niigata University), Prof. Noboru Ono (Kyoto University), and Prof. Chad A. Mirkin (Northwestern University) for the collaborative works in development of new polymers and nanorods.

References

1. G. Li, R. Zhu and Y. Yang, *Nat. Photonics*, 2012, **6**, 153–161.
2. F. He and L. Yu, *J. Phys. Chem. Lett.*, 2011, **2**, 3102–3113.
3. B. C. Thompson and Jean M. J. Fréchet, *Angew. Chem. Int. Ed.*, 2008, **47**, 58–77.
4. M. Hiramoto, H. Fujiwara and M. Yokoyama, *Appl. Phys. Lett.*, 1991, **58**, 1062–1064.
5. G. Yu, J. Gao, J. C. Hummelen, F. Wudl and A. J. Heeger, *Science*, 1995, **270**, 1789–1791.
6. K. Vandewal, S. Himmelberger and A. Salleo, *Macromolecules*, 2013, **46**, 6379–6387.
7. L.-M. Chen, Z. Xu, Z. Hong and Y. Yang, *J. Mater. Chem.*, 2010, **20**, 2575–2598.
8. G. Li, C.-W. Chu, V. Shrotriya, J. Huang and Y. Yang, *Appl. Phys. Lett.*, 2006, **88**, 253503.
9. T. Ameri, G. Dennler, C. Waldauf, H. Azimi, A. Seemann, K. Forberich, J. Hauch, M. Scharber, K. Hingerl and C. J. Brabec, *Adv. Funct. Mater.*, 2010, **20**, 1592–1598.
10. T. Kuwabara, Y. Kawahara, T. Yamaguchi and K. Takahashi, *ACS Appl. Mater. Interfaces*, 2009, **1**, 2107–2110.
11. C. E. Small, S. Chen, J. Subbiah, C. M. Amb, S.-W. Tsang, T.-H. Lai, J. R. Reynolds and F. So, *Nat. Photonics*, 2012, **6**, 115–120.
12. Z. He, C. Zhong, S. Su, M. Xu, H. Wu and Y. Cao, *Nat. Photonics*, 2012, **6**, 591–595.
13. S. Liu, K. Zhang, J. Lu, J. Zhang, H.-L. Yip, F. Huang and Y. Cao, *J. Am. Chem. Soc.*, 2013, **135**, 15326–15329.
14. J. You, L. Dou, K. Yoshimura, T. Kato, K. Ohya, T. Moriarty, K. Emery, C.-C. Chen, J. Gao, G. Li and Y. Yang, *Nat. Commun.*, 2013, **4**, 1446.
15. X. Guo, N. Zhou, S. J. Lou, J. Smith, D. B. Tice, J. W. Hennek, R. P. Ortiz, J. T. L. Navarrete, S. Li, J. Strzalka, L. X. Chen, R. P. H. Chang, A. Facchetti and T. J. Marks, *Nat. Photonics*, 2013, **7**, 825–833.
16. M. S. Scharber, D. Mühlbacher, M. Koppe, P. Denk, C. Waldauf, A. J. Heeger and C. J.

Brabec, *Adv. Mater.*, 2006, **18**, 789–794.

17. B. Qi and J. Wang, *J. Mater. Chem.*, 2012, **22**, 24315–24325.
18. B. Qi and J. Wang, *Phys. Chem. Chem. Phys.*, 2013, **15**, 8972–8982.
19. M.-S. Kim, B.-G. Kim and J. Kim, *ACS Appl. Mater. Int.*, 2009, **1**, 1264–1269.
20. Z. He, C. Zhong, X. Huang, W.-Y. Wong, H. Wu, L. Chen, S. Su and Y. Cao, *Adv. Mater.*, 2011, **23**, 4636–4643.
21. H.-C. Chen, Y.-H. Chen, C.-C. Liu, Y.-C. Chien, S.-W. Chou and P.-T. Chou, *Chem. Mater.*, 2012, **24**, 4766–4772.
22. C. Duan, K. Zhang, X. Guan, C. Zhong, H. Xie, F. Huang, J. Chen, J. Peng and Y. Cao, *Chem. Sci.*, 2013, **4**, 1298–1307.
23. L. Dou, C.-C. Chen, K. Yoshimura, K. Ohya, W.-H. Chang, J. Gao, Y. Liu, E. Richard and Y. Yang, *Macromolecules*, 2013, **46**, 3384–3390.
24. C. Cabanetos, A. E Labban, J. A. Bartelt, J. D. Douglas, W. R. Mateker, J. M. J. Fréchet, M. D. McGehee and P. M. Beaujuge, *J. Am. Chem. Soc.*, 2013, **135**, 4656–4659.
25. I. Osaka, T. Kakara, N. Takemura, T. Koganezawa and K. Takimiya, *J. Am. Chem. Soc.*, 2013, **135**, 8834–8837.
26. I. Y. Kanal, S. G. Owens, J. S. Bechtel and G. R. Hutchison, *J. Phys. Chem. Lett.*, 2013, **4**, 1613–1623.
27. H. Zhou, L. Yang and W. You, *Macromolecules*, 2012, **45**, 607–632.
28. R. L. Uy, S. C. Price and W. You, *Macromol. Rapid Commun.*, 2012, **33**, 1162–1177.
29. Z. G. Zhang and J. Wang, *J. Mater. Chem.*, 2012, **22**, 4178–4187.
30. P. M. Beaujuge and J. M. J. Fréchet, *J. Am. Chem. Soc.*, 2011, **133**, 20009–20029.
31. G. Yu, J. Gao, J. C. Hummelen, F. Wudl and A. J. Heeger, *Science*, 1995, **270**, 1789–1791.
32. Y. He, H.-Y. Chen, J. Hou and Y. Li, *J. Am. Chem. Soc.*, 2010, **132**, 1377–1382.

33. C. L. Chochos, N. Tagmatarchis and V. G. Gregoriou, *RSC Adv.*, 2013, **3**, 7160–7181.

34. C.-Z. Li, H.-L. Yip and A. K.-Y. Jen, *J. Mater. Chem.*, 2012, **22**, 4161–4177.

35. Y. He and Y. Li, *Phys. Chem. Chem. Phys.*, 2011, **13**, 1970–1983.

36. K. Vandewal, S. Himmelberger and A. Salleo, *Macromolecules*, 2013, **46**, 6379–6387.

37. M. Pfannmöller, W. Kowalsky and R. R. Schröder, *Energy Environ. Sci.*, 2013, **6**, 2871–2891.

38. C. J. Brabec, M. Heeney, I. McCulloch and J. Nelson, *Chem. Soc. Rev.*, 2011, **40**, 1185–1199.

39. N. D. Treat, A. Varotto, C. J. Takacs, N. Batara, M. Al-Hashimi, M. J. Heeney, A. J. Heeger, F. Wudl, C. J. Hawker and M. L. Chabinyc, *J. Am. Chem. Soc.*, 2012, **134**, 15869–15879.

40. H. Imahori, K. Hagiwara, T. Akiyama, M. Aoki, S. Taniguchi, T. Okada, M. Shirakawa and Y. Sakata, *Chem. Phys. Lett.*, 1996, **263**, 545–550.

41. H. Imahori, *Bull. Chem. Soc. Jpn.*, 2007, **80**, 621–636.

42. J. Peet, J. Y. Kim, N. E. Coates, W. L. Ma, D. Moses, A. J. Heeger and G. C. Bazan, *Nat. Chem.*, 2007, **6**, 497–500.

43. F. Padinger, R. S. Rittberger and N. S. Sariciftci, *Adv. Funct. Mater.*, 2003, **13**, 85–88.

44. S. B. Jo, W. H. Lee, L. Qiu and K. Cho, *J. Mater. Chem.*, 2012, **22**, 4216–4232.

45. T. Song, S.-T. Lee and B. Sun, *J. Mater. Chem.*, 2012, **22**, 4244–4260.

46. S.-S. Li and C.-W. Chen, *J. Mater. Chem. A*, 2013, **1**, 10574–10591.

47. F. Wudl, M. Kobayashi and A. J. Heeger, *J. Org. Chem.*, 1984, **49**, 3382–3384.

48. M. Kobayashi, N. Colaneri, M. Boysel, F. Wudl, and A. J. Heeger, *J. Chem. Phys.*, 1985, **82**, 5717–5723.

49. K. Nayak and D. S. Marynick, *Macromolecules*, 1990, **23**, 2237–2245.

50. M. Pomerantz, B. Chaloner-Gill, L. O. Harding, J. J. Tseng and W. J. Pomerantz, *J. Chem. Soc., Chem. Commun.*, 1992, 1672–1673.

51. G. A. Sotzing and K. Lee, *Macromolecules*, 2002, **35**, 7281–7286.

52. H. Zhou, L. Yang and W. You, *Macromolecules*, 2012, **45**, 607–632.

53. H.-Y. Chen, J. Hou, S. Zhang, Y. Liang, G. Yang, Y. Yang, L. Yu, Y. Wu and G. Li, *Nat. Photonics*, 2009, **3**, 649–653.

54. Y. Liang, Z. Xu, J. Xia, S.-T. Tsai, Y. Wu, G. Li, C. Ray and L. Yu, *Adv. Mater.*, 2010, **22**, E135–E138.

55. H. J. Son, W. Wang, T. Xu, Y. Liang, Y. Wu, G. Li and L. Yu, *J. Am. Chem. Soc.*, 2011, **133**, 1885–1894.

56. R. S. Kularatne, H. D. Magurudeniya, P. Sista, M. C. Biewer and M. C. Stefan, *J. Polym. Sci. A: Polym. Chem.*, 2013, **51**, 743–768.

57. M. Mayukh, I. H. Jung, F. He and L. Yu, *J. Polym. Sci. B: Polym. Phys.*, 2012, **50**, 1057–1070.

58. J. M. Szarko, J. Guo, B. S. Rolczynski and L. X. Chen, *J. Mater. Chem.*, 2011, **21**, 7849–7857.

59. Y. Liang and L. Yu, *Polym. Rev.*, 2010, **50**, 454–473.

60. D. L. Vangeneugden, D. J. M. Vanderzande, J. Salbeck, P. A. van Hal, R. A. J. Janssen, J. C. Hummelen, C. J. Brabec, S. E. Shaheen and N. S. Sariciftci, *J. Phys. Chem. B*, 2001, **105**, 11106–11113.

61. S. E. Shaheen, D. Vangeneugden, R. Kiebooms, D. Vanderzande, T. Fromherz, F. Padinger, C. J. Brabec and N. S. Sariciftci, *Synth. Met.*, 2001, **121**, 1583–1584.

62. J. Y. Kim, Y. Qin, D. M. Stevens, V. Kalihari, M. A. Hillmyer and C. D. Frisbie, *J. Phys. Chem. C*, 2009, **113**, 21928–21936.

63. Y. Qin, J. Y. Kim, C. D. Frisbie and M. A. Hillmyer, *Macromolecules*, 2008, **41**, 5563–5570.

64. L. Huo and J. Hou, *Polym. Chem.*, 2011, **2**, 2453–2461.

65. Y. Shimizu, Z. Shen, S. Ito, H. Uno, J. Daub and N. Ono, *Tetrahedron Lett.*, 2002, **43**, 8485–8488.

66. H. Yamada, T. Okujima and N. Ono, *Chem. Commun.*, 2008, 2957–2974.

67. T. Umeyama, K. Hirose, K. Noda, K. Matsushige, T. Shishido, H. Hayashi, Y. Matano, N. Ono and H. Imahori, *J. Phys. Chem. C*, 2012, **116**, 1256–1264.

68. T. Umeyama, K. Hirose, K. Noda, K. Matsushige, T. Shishido, H. Saarenpää, N. V. Tkachenko, H. Lemmetyinen, N. Ono and H. Imahori, *J. Phys. Chem. C*, 2012, **116**, 17414–17423.

69. M. R. Raj and S. Anandana, *RSC Adv.*, 2013, **3**, 14595–14608.

70. J. D. Douglas, G. Griffini, T. W. Holcombe, E. P. Young, O. P. Lee, M. S. Chen and J. M. J. Fréchet, *Macromolecules*, 2012, **45**, 4069–4074.

71. G. Long, X. Wan, J. Zhou, Y. Liu, Z. Li, G. He, M. Zhang, Y. Hou and Y. Chen, *Macromol. Chem. Phys.*, 2012, **213**, 1596–1603.

72. H. Li, S. Sun, T. Salim, S. Bomma, A. C. Grimsdale and Y. M. Lam, *J. Polym. Sci. A: Polym. Chem.*, 2012, **50**, 250–260.

73. W. A. Braunecker, Z. R. Owczarczyk, A. Garcia, N. Kopidakis, R. E. Larsen S. R. Hammond, D. S. Ginley and D. C. Olson, *Chem. Mater.*, 2012, **24**, 1346–1356.

74. Y. Wu, Y. Jing, X. Guo, S. Zhang, M. Zhang, L. Huoa and J. Hou, *Polym. Chem.*, 2013, **4**, 536–541.

75. Y. P. Zou, A. Najari, P. Berrouard, S. Beaupre, B. R. Aich, Y. Tao and M. Leclerc, *J. Am. Chem. Soc.*, 2010, **132**, 5330–5331.

76. C. Piliego, T. W. Holcombe, J. D. Douglas, C. H. Woo, P. M. Beaujuge and J. M. J. Fréchet, *J. Am. Chem. Soc.*, 2010, **132**, 7595–7597.

77. T. Umeyama, M. Odoi, O. Yoshikawa, T. Sagawa, S. Yoshikawa, D. Evgenia, N. Tezuka, Y. Matano, K. Stranius, N. V. Tkachencko, H. Lemmetyinen and H. Imahori, *J. Mater. Chem.*, 2011, **21**, 12454–12461.

78. A. Pron, P. Berrouard and M. Leclerc, *Macromol. Chem. Phys.*, 2013, **214**, 7–16.

79. H. Meng and F. Wudl, *Macromolecules*, 2001, **34**, 1810–1816.

80. H. Li, S. Sun, T. Salim, S. Bomma, A. C. Grimsdale and Y. M. Lam, *J. Polym. Sci. A: Polym. Chem.*, 2012, **50**, 250–260.

81. W. A. Braunecker, Z. R. Owczarczyk, A. Garcia, N. Kopidakis, R. E. Larsen S. R. Hammond, D. S. Ginley and D. C. Olson, *Chem. Mater.*, 2012, **24**, 1346–1356.

82. Y. Wu, Y. Jing, X. Guo, S. Zhang, M. Zhang, L. Huoa and J. Hou, *Polym. Chem.*, 2013, **4**, 536–541.

83. S. A. Jenekhe, *Nature*, 1986, **322**, 345–347.

84. W.-C. Chen and S. A. Jenekhe, *Macromolecules*, 1995, **28**, 454–464.

85. A. O. Patil and F. Wudl, *Macromolecules*, 1988, **21**, 540–542.

86. H. Bräunling, R. Becker and G. Blöchl, *Synth. Met.*, 1991, **42**, 1539–1547.

87. W.-C. Chen and S. A. Jenekhe, *Macromol. Chem. Phys.*, 1998, **199**, 655–666.

88. T. Umeyama, Y. Watanabe, M. Oodoi, D. Evgenia, T. Shishido and H. Imahori, *J. Mater. Chem.*, 2012, **22**, 24394–24402.

89. Y. Li, P. Sonar, L. Murphy and W. Hong, *Energy Environ. Sci.*, 2013, **6**, 1684–1710

90. L. Dou, W.-H. Chang, J. Gao, C.-C. Chen, J. You and Y. Yang, *Adv. Mater.*, 2013, **25**, 825–831.

91. J. J. Intemann, K. Yao, H.-L. Yip, Y.-X. Xu, Y.-X. Li, P.-W. Liang, F.-Z. Ding, X. Li and A. K.-Y. Jen, *Chem. Mater.*, 2013, **25**, 3188–3195.

92. T.-Y. Chu, J. Lu, S. Beaupré, Y. Zhang, J.-R. Pouliot, S. Wakim, J. Zhou, M. Leclerc, Z. Li, J. Ding and Y. Tao, *J. Am. Chem. Soc.*, 2011, **133**, 4250–4253.

93. C. M. Amb, S. Chen, K. R. Graham, J. Subbiah, C. E. Small, F. So and J. R. Reynolds, *J. Am. Chem. Soc.*, 2011, **133**, 10062–10065.

94. H.-Y. Chen, S.-C. Yeh, C.-T. Chen and C.-T. Chen, *J. Mater. Chem.*, 2012, **22**, 21549–21559.

95. Y. Matano and H. Imahori, *Org. Biomol. Chem.*, 2009, **7**, 1258–1271.

96. M. Sebastian, M. Hissler, C. Fave, J. Rault-Berthelot, C. Odin and R. Réau, *Angew. Chem. Int. Ed.*, 2006, **45**, 6152–6155.

97. T. Baumgartner, W. Bergmans, T. Kárpáti, T. Neumann, M. Nieger and L. Nyulászi, *Chem. Eur. J.*, 2005, **11**, 4687–4699.

98. A. Saito, Y. Matano and H. Imahori, *Org. Lett.*, **2010**, *12*, 2675–2677.

99. Y. Matano, H. Ohkubo, Y. Honsho, A. Saito, S. Seki and H. Imahori, *Org. Lett.*, **2013**, *15*, 932–935.

100. Y. Matano, H. Ohkubo, T. Miyata, Y. Watanabe, Y. Hayashi, T. Umeyama and H. Imahori, *Eur. J. Inorg. Chem.*, **2013**, DOI:10.1002/ejic.201301132.

101. M. R. Wasielewski, *Chem. Rev.* **1992**, *92*, 435–461.

102. H. Imahori, H. Yamada, D. M. Guldi, Y. Endo, A. Shimomura, S. Kundu, K. Yamada, T. Okada, Y. Sakata and S. Fukuzumi, *Angew. Chem. Int. Ed.*, **2002**, *41*, 2344–2347.

103. A. Yella, H.-W. Lee, H. N. Tsao, C. Yi, A. K. Chandiran, M. K. Nazeeruddin, E. W.-G. Diau, C.-Y. Yeh, S. M. Zakeeruddin and M. Grätzel, *Science*, 2011, **334**, 629–634.

104. K. Kurotobi, Y. Toude, K. Kawamoto, Y. Fujimori, S. Ito, P. Chabera, V. Sundström and H. Imahori, *Chem. Eur. J.*, **2013**, *19*, 17075–17081.

105. H. Imahori, T. Umeyama and S. Ito, *Acc. Chem. Res.*, **2009**, *42*, 1809–1818.

106. X. Huang, C. Zhu, S. Zhang, W. Li, Y. Guo, X. Zhan, Y. Liu and Z. Bo, *Macromolecules*, **2008**, *41*, 6895–6902.

107. T. Umeyama, T. Takamatsu, N. Tezuka, Y. Matano, Y. Araki, T. Wada, O. Yoshikawa, T. Sagawa, S. Yoshikawa and H. Imahori, *J. Phys. Chem. C*, **2009**, *113*, 10798–10806.

108. N. Xiang, Y. Liu, W. Zhou, H. Huang, X. Guo, Z. Tan, B. Zhao, P. Shen and S. Tan, *Eur. Polym. J.*, **2010**, *46*, 1084–1092.

109. J. Y. Lee, H. J. Song, S. M. Lee, J. H. Lee and D. K. Moon, *Eur. Polym. J.*, **2011**, *47*, 1686–1693.

110. W. Zhou, P. Shen, B. Zhao, P. Jiang, L. Deng and S. Tan, *J. Polym. Sci. A: Polym. Chem.*, **2011**, *49*, 2685–2692.

111. H. Zhan, S. Lamare, A. Ng, T. Kenny, H. Guernon, W.-K. Chan, A. B. Djurišić, P. D. Harvey and W.-Y. Wong, *Macromolecules*, **2011**, *44*, 5155–5167.

112. S. Shi, X. Wang, Y. Sun, S. Chen, X. Li, Y. Li and H. Wang, *J. Mater. Chem.*, **2012**, *22*, 11006–11008.

113. S. Shi, P. Jiang, S. Chen, Y. Sun, X. Wang, K. Wang, S. Shen, X. Li, Y. Li and H. Wang, *Macromolecules*, **2012**, *45*, 7806–7814.

114. H. Zhou, L. Yang, A. C. Stuart, S. C. Price, S. Liu and W. You, *Angew. Chem. Int. Ed.*, 2011, **50**, 2995–2998.

115. A. C. Stuart, J. R. Tumbleston, H. Zhou, W. Li, S. Liu, H. Ade and W. You, *J. Am. Chem. Soc.*, 2013, **135**, 1806–1815.

116. C.-Y. Chang, L. Zuo, H.-L Yip, Y. Li, C.-Z. Li, C.-S. Hsu, Y.-J. Cheng, H. Chen and A. K.-Y. Jen, *Adv. Funct. Mater.*, 2013, **23**, 5084–5090.

117. D. Dang, W. Chen, R. Yang, W. Zhu, W. Mammod and E. Wang, *Chem. Commun.*, 2013, **49**, 9335–9337.

118. S. C. Price, A. C. Stuart, L. Yang, H. Zhou and W. You, *J. Am. Chem. Soc.*, 2011, **133**, 4625–4631.

119. A. Cardone, C. Martinelli, M. Losurdo, E. Dilonardo, G. Bruno, G. Scavia, S. Destri, P. Cosma, L. Salamandra, A. Reale, A. D. Carlo, A. Aguirre, B. Milián-Medina, J. Gierschner and G. M. Farinola, *J. Mater. Chem. A*, 2013, **1**, 715–727.

120. N. Blouin, A. Michaud and M. Leclerc, *Adv. Mater.*, 2007, **19**, 2295–2300.

121. S. H. Park, A. Roy, S. Beaupre, S. Cho, N. Coates, J. S. Moon, D. Moses, M. Leclerc, K. Lee and A. J. Heeger, *Nat. Photonics*, 2009, **3**, 297–303.

122. S. Beaupré and M. Leclerc, *J. Mater. Chem. A*, 2013, **1**, 11097–11105.

123. M. F. G. Klein, F. M. Pasker, S. Kowarik, D. Landerer, M. P. M. Isen, D. Gerthsen, U. Lemmer, S. Höger and A. Colsmann, *Macromolecules*, 2013, **46**, 3870–3878.

124. E. Wang, L. Hou, Z. Wang, Z. Ma, S. Hellström, W. Zhuang, F. Zhang, O. Inganäs and M. R. Andersson, *Macromolecules*, 2011, **44**, 2067–2073.

125. T. Umeyama, Y. Watanabe, E. Douvogianni and H. Imahori, *J. Phys. Chem. C*, 2013, **117**, 21148–21157.

126. C. Shim, M. Kim, S.-G. Ihn, Y. S. Choi, Y. Kim and K. Cho, *Chem. Commun.*, 2012, **48**, 7206–7208.

127. F. Etzold, I. A. Howard, N. Forler, D. M. Cho, M. Meister, H. Mangold, J. Shu, M. R. Hansen, K. Müllen and F. Laquai, *J. Am. Chem. Soc.*, 2012, **134**, 10569–10583.

128. Y. H. Huh and B. Park, *Opt. Express*, 2013, **21**, A146–A156.

129. M. N. Chaur, F. Melin, A. L. Ortiz and L. Echegoyen, *Angew. Chem., Int. Ed.*, 2009, **48**, 7514–7538.

130. R. B. Ross, C. M. Cardona, D. M. Guldi, S. G. Sankaranarayanan, M. O. Reese, N. Kopidakis, J. Peet, B. Walker, G. C. Bazan, E. Van Keuren, B. C. Holloway and M. Drees, *Nat. Mater.*, 2009, **8**, 208–212.

131. J. M. Frost, M. A. Faist and J. Nelson, *Adv. Mater.*, 2010, **22**, 4881–4884.

132. M. Lens, G.-J. A. H. Wetzelaer, F. B. Kooistra, S. C. Veenstra, J. C. Hummelen and P. W. M. Blom, *Adv. Mater.*, 2008, **20**, 2116–2119.

133. Y. He, H.-Y. Chen, J. Hou and Y. Li, *J. Am. Chem. Soc.*, 2010, **132**, 1377–1382.

134. S.-H. Liao, Y.-L. Li, T.-H. Jen, Y.-S. Cheng and S.-A. Chen, *J. Am. Chem. Soc.*, 2012, **134**,

14271–14274.

135. Y.-J. Cheng, M.-H. Liao, C.-Y. Chang, W.-S. Kao, C.-E. Wu and C.-S. Hsu, *Chem. Mater.*, 2011, **23**, 4056–4062.

136. C. Zhang, S. Chen, Z. Xiao, Q. Zuo and L. Ding, *Org. Lett.*, 2012, **14**, 1508–1511.

137. Z. Xiao, Y. Matsuo, I. Soga and E. Nakamura, *Chem. Mater.*, 2012, **24**, 2572–2582.

138. S. Kitaura, K. Kurotobi, M. Sato, Y. Takano, T. Umeyama and H. Imahori, *Chem. Commun.*, 2012, **48**, 8550–8552.

139. A. Hirsch, I. Lamparth and H. R. Karfunkel, *Angew. Chem. Int. Ed.*, 1994, **33**, 437–438.

140. D. S. Sabirov, *J. Phys. Chem. C*, 2013, **117**, 9148–9153.

141. X. Meng, W. Zhang, Z. Tan, C. Du, C. Li, Z. Bo, Y. Li, X. Yang, M. Zhen, F. Jiang, J. Zheng, T. Wang, L. Jiang, C. Shu and C. Wang, *Chem. Commun.*, 2012, **48**, 425–427.

142. X. Meng, G. Zhao, Q. Xu, Z. Tan, Z. Zhang, L. Jiang, C. Shu, C. Wang and Y. Li, *Adv. Funct. Mater.*, 2014, **24**, 158–163.

143. Y. Qu and X. Duan, *J. Mater. Chem.*, 2012, **22**, 16171–16181.

144. E. C. Garnett, M. L. Brongersma, Y. Cui and M. D. McGehee, *Annu. Rev. Mater. Res.*, 2011, **41**, 269–295.

145. Y. Zhang, H. Dong, Q. Tang, S. Ferdous, F. Liu, S. C. B. Mannsfeld, W. Hu and A. L. Briseno, *J. Am. Chem. Soc.*, 2010, **132**, 11580–11584.

146. H. Imahori, S. Kitaura, A. Kira, H. Hayashi, M. Nishi, K. Hirao, S. Isoda, M. Tsujimoto, M. Takano, Z. Zhe, Y. Miyato, K. Noda, K. Matsushige, K. Stranius, N. V. Tkachenko, H. Lemmetyinen, L. Qin, S. J. Hurst and C. A. Mirkin, *J. Phys. Chem. Lett.*, 2012, **3**, 478–481.

147. Q. H. Cui, L. Jiang, C. Zhang, Y. S. Zhao, W. Hu and J, Yao, *Adv. Mater.*, 2012, **24**, 2332–2336.

148. J. Tan, L. Jiang, L. He, H. Dong and W. Hu, *Appl. Phys. Lett.*, 2012, **100**, 173902.

149. L. Jiang, J. Gao, E. Wang, H. Li, Z. Wang, W. Hu and L. Jiang, *Adv. Mater.*, 2008, **20**, 2735–2740.

150. G. Yu, J. Gao, J. C. Hummelen, F. Wudl and A. J. Heeger, *Science*, 1995, **270**, 1789–1791.

151. R. A. J. Janssen and J. Nelson, *Adv. Mater.*, 2013, **25**, 1847–1858.

152. P. K. Nayak, K. L. Narasimhan and D. Cahen, *J. Phys. Chem. Lett.*, 2013, **4**, 1707–1717.

153. G. Grancini, M. Maiuri, D. Fazzi, A. Petrozza, H.-J. Egelhaaf, D. Brida, G. Cerullo and G. Lanzani, *Nat. Mater.*, 2013, **12**, 29–33.

154. A. E. Jailaubekov, A. P. Willard, J. R. Tritsch, W.-L. Chan, N. Sai, R. Gearba, L. G. Kaake, K. J. Williams, K. Leung, P. J. Rossky and X.-Y. Zhu, *Nat. Mater.*, 2013, **12**, 66–73.

155. A. Rao, P. C. Y. Chow, S. Gélinas, C. W. Schlenker, C.-Z. Li, H.-L. Yip, A. K.-Y. Jen, D. S. Ginger and R. H. Friend, *Nature*, 2013, **500**, 435–440.

Table 1 Molecular weights, bandgaps, HOMO energy levels, and photovoltaic properties of polymers in Fig. 3.

polymer	M_n / kg mol^{-1}	E_g / eV	HOMO / eV	J_{SC} / mA cm^{-2}	V_{OC} / V	*FF*	PCE / %	ref
P1	5.7	1.55	–5.3	3.4	0.83	0.32	0.90	57
P2	10[a]	1.3	–5.3	2.41	0.42	0.29	0.29	63
P3	398	1.86	–5.56	4.89	0.74	0.55	1.98	64
P4a	24	1.60	–5.59	6.70	0.88	0.47	2.74	65
P4b	27.5	1.52	–5.30	5.90	0.64	0.33	1.25	66
P5a	43	1.57	–5.69	8.63	0.76	0.46	3.04	65
P5b	40.3	1.43	–5.37	5.0	0.79	0.52	2.1	76
P6	20	1.53	–5.52	6.50	0.80	0.60	3.12	77
P7a	4.7	1.2	–5.2	6.58	0.53	0.42	1.44	83
P7b	8.2	1.2	–4.9	5.58	0.45	0.41	0.96	83

[a] M_n of precursor polymer **P-P2**.

Table 2 LUMO levels of **F3** – **F5** and PSC device characteristics[a] based on P3HT: **F3** – **F5**.

Acceptor	LUMO / eV	J_{SC} / mA cm^{-2}	V_{OC} / V	*FF*	PCE / %
F3 *trans*-1	–3.91	1.43	0.29	0.30	0.12
F3 *trans*-2	–3.84	4.73	0.73	0.40	1.38
F3 *trans*-3	–3.78	3.57	0.65	0.39	0.89
F3 *trans*-4	–3.78	4.63	0.71	0.44	1.44
F3 *e*	–3.78	4.56	0.70	0.44	1.41
F3 *cis*-2 + *cis*-3	–3.80	3.44	0.57	0.31	0.62
F3 mixture	–3.86	3.71	0.68	0.38	0.95
F4	–3.96	5.14	0.66	0.50	1.71
F5 *trans*-2	–3.76	10.04	0.83	0.69	5.8
F5 *trans*-3	–3.70	10.21	0.88	0.71	6.3
F5 *trans*-4	–3.72	9.67	0.86	0.67	5.6
F5 *e*	–3.73	9.51	0.86	0.67	5.5
F5 mixture	–3.76	9.88	0.82	0.67	5.3

[a]The PSC device structures are ITO/PEDOT:PSS/P3HT:fullerene/Al for **F3** and **F4** and ITO/PEDOT:PSS/P3HT:fullerene/Ca/Al for **F5**.

Scheme 1 Thermal conversion of **P-P2** to **P2**.

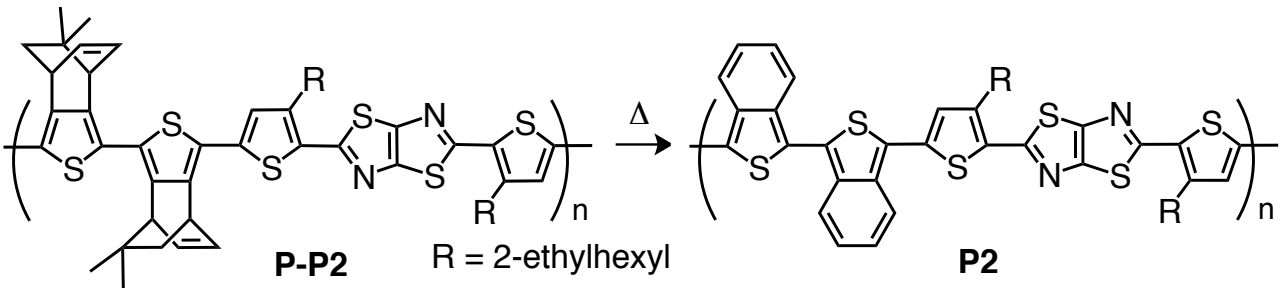

Scheme 2 Template synthesis of nanorods.

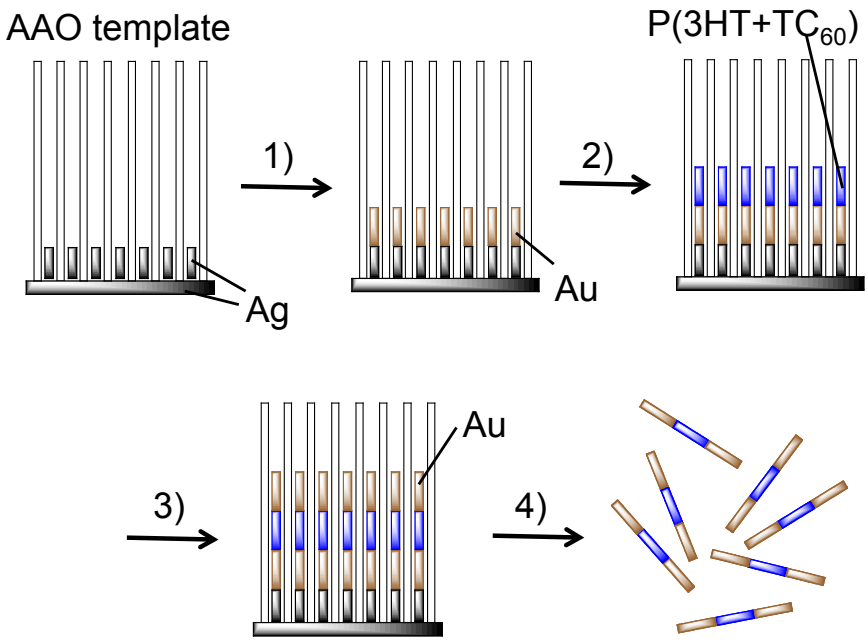

1) Electrodeposition of Au. 2) Electrochemical copolymerization of 3HT and TC_{60}. 3) Electrodeposition of Au. 4) Dissolution of Ag film with conc. HNO_3, then dissolution of AAO template with 3M NaOH aq.

Scheme 3 Electrochemical polymerization of 3HT and TC_{60}.

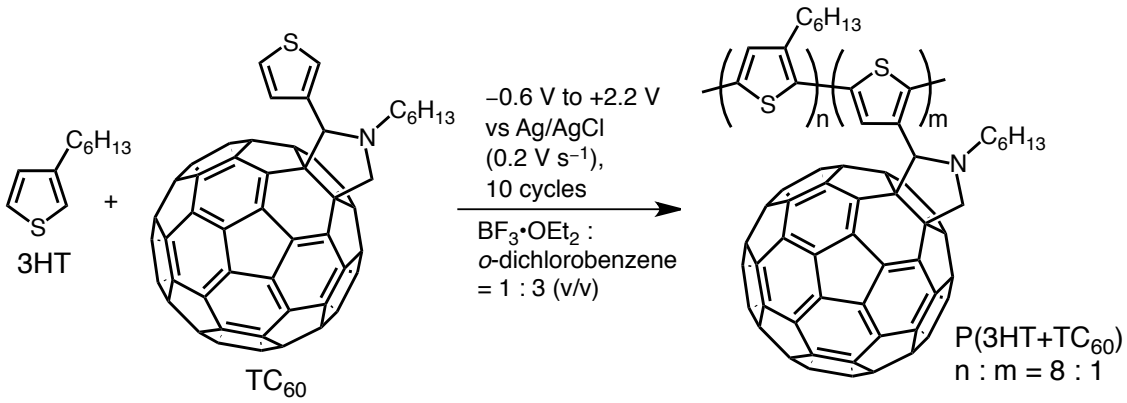

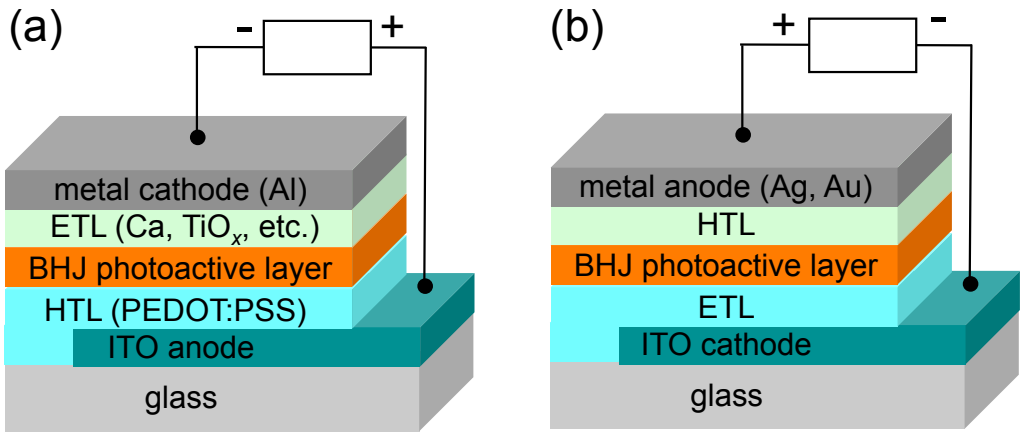

Fig. 1 PSC device structures with (a) conventional and (b) inverted configurations. HTL: hole transporting layer, ETL: electron transporting layer.

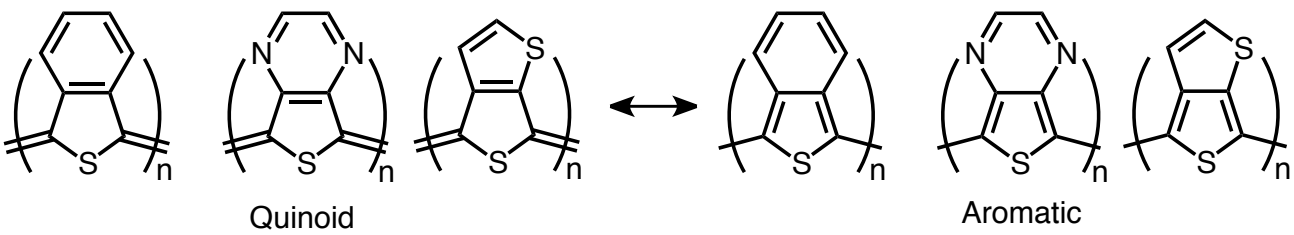

Fig. 2 Quinoid and aromatic forms of poly(isothianaththene), poly(thieno[3,4-*b*]pyrazine) and poly(thieno[3,4-*b*]thiophene).

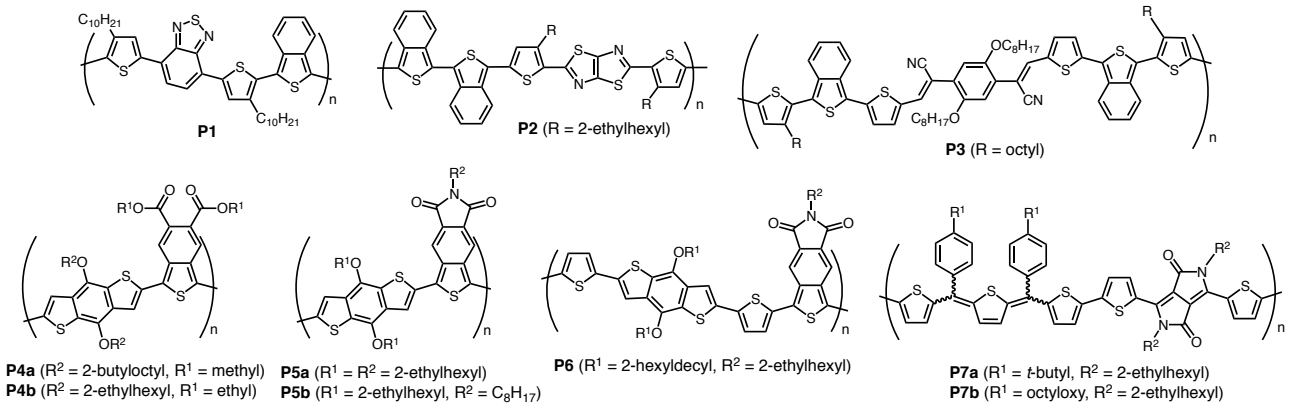

Fig. 3 Structures of quinoid conjugated polymers.

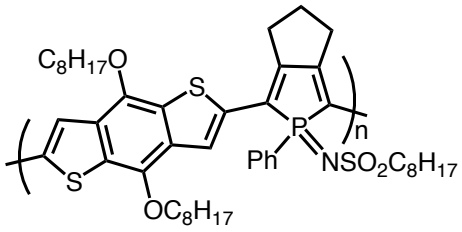

P8a
(M_n = 13800, HOMO = –5.65 eV,
E_g = 1.73 eV, PCE = 0.07%)

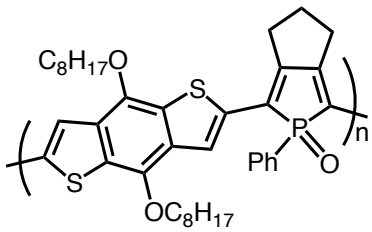

P8b
(M_n = 11500, HOMO = –5.32 eV,
E_g = 1.69 eV, PCE = 0.65%)

Fig. 4 Structures of phosphole-based conjugated polymers.

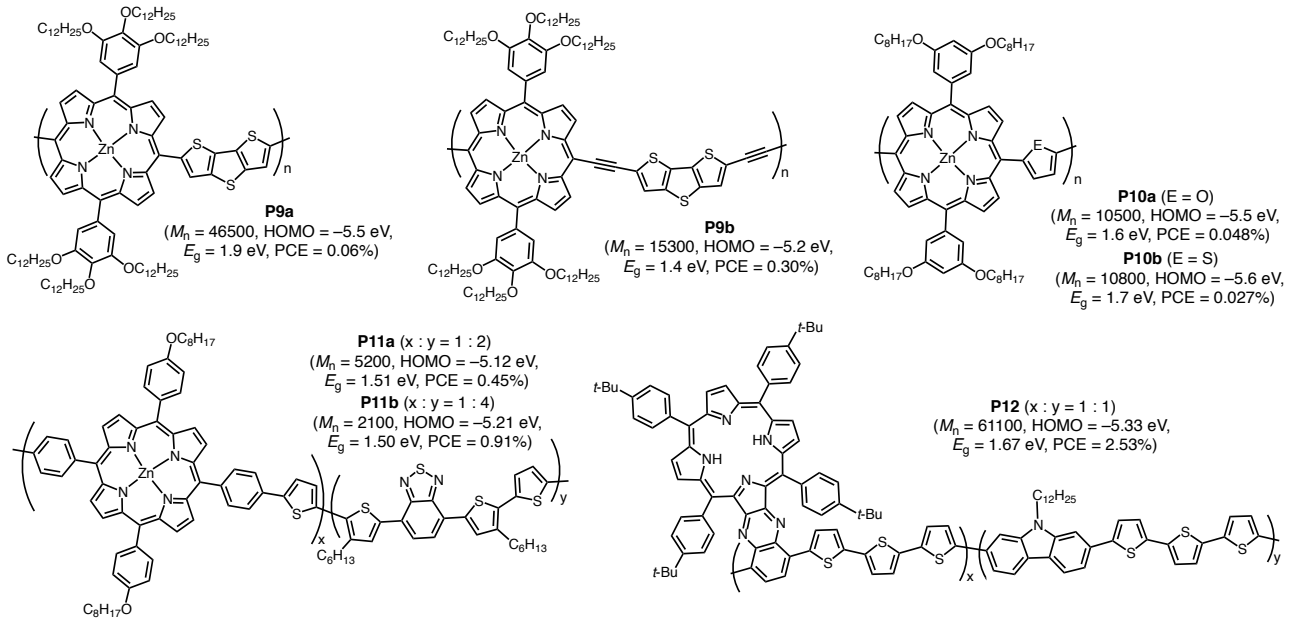

Fig. 5 Structures of porphyrin-based conjugated polymers.

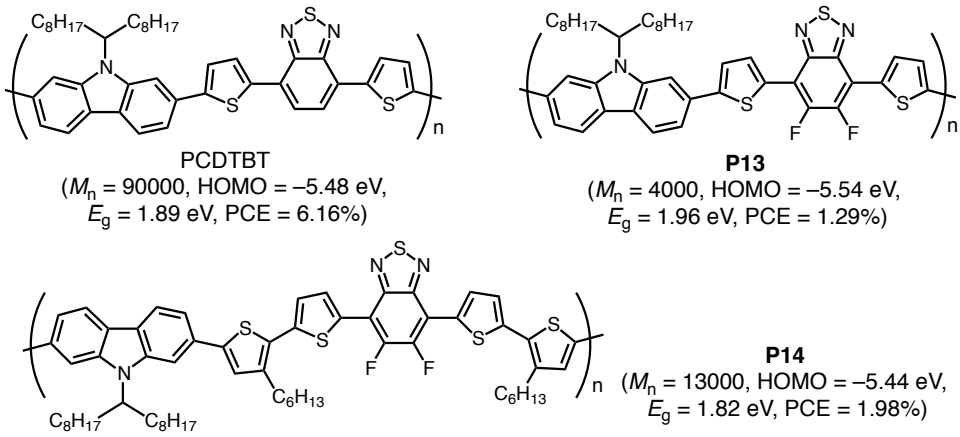

Fig. 6 Structures of PCDTBT and its fluorinated analogues. The data of PCDTBT in parenthesis are extracted from reference 125.

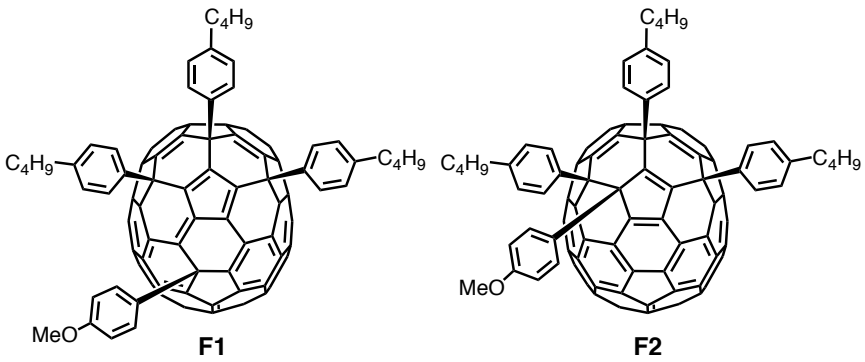

Fig. 7 Structures of **F1** and **F2**.

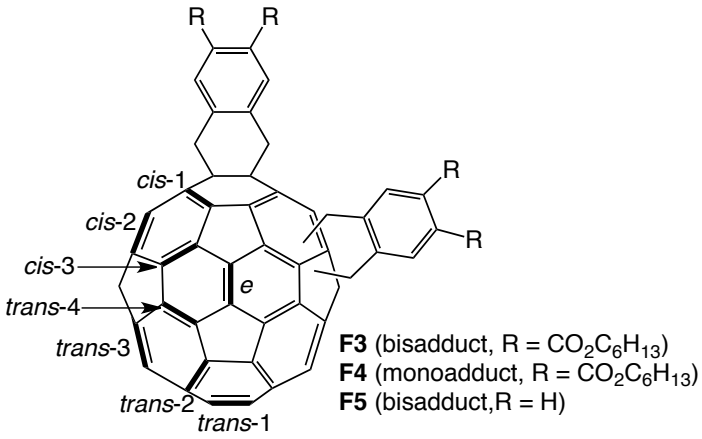

Fig. 8 Structures of **F3**, **F4** and **F5** with the possible regioisomers.

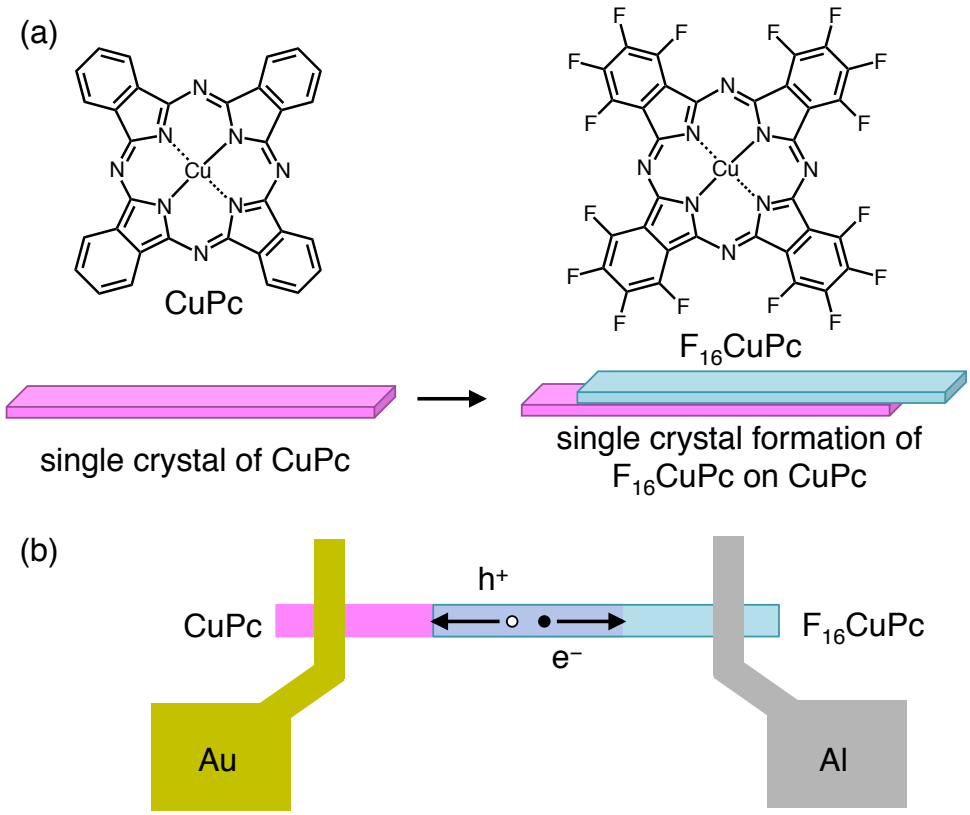

Fig. 9 (a) Structures and illustration of nanoribbon crystals of CuPc and F_{16}CuPc. (b) Schematic illustration of a discrete D−A heterojunction photovoltaic device.